
The salt intrusion response of morphodynamic estuaries to changing river discharge

MSc Thesis

Meike Traas

Student number: 6994008

Supervisors:

Dr. ir. Jaap Nienhuis

Dr. Maarten van der Vegt

Master: Earth Surface and Water

Track: Coastal Dynamics and Fluvial Systems

Credits: 37.5 ECTS

Department of Physical Geography

Universiteit Utrecht

The Netherlands

March 18, 2022

Abstract

Salt intrusion has large consequences on the estuarine environments and communities. Salinization harms the ecology and biodiversity in an estuary and it might constrain the possibilities of using water for irrigation, industry and human consumption. Due to the seasons, climate change and increasing anthropogenic influences, the river discharge might change on short or long timescales which will affect the salt intrusion and the morphology on the long term. Previous research has been done to the effect of river discharge on salt intrusion, but those use a morphostatic model with a constant width profile. In this thesis, a one-dimensional tide-averaged numerical hydrodynamic and morphodynamic model is used, which includes a variable width and a constant bed level. This model is best suitable to simulate the response of estuaries globally, and less suitable to look into details for individual estuary systems. The estuary width is calculated by an optimized empirical hydraulic geometry relation that relates the width to the river discharge and tidal peak discharge. River discharge and tides force the upstream and downstream boundaries, respectively. For the salt intrusion length, an empirical method was used after validation. On the short term, the morphology of an estuary will not change, meaning that only the hydrodynamics can affect the salt intrusion length. This results in higher salt intrusion lengths for lower river discharges, since the tide is less countered by friction with the river flow. On the long term, the estuary will narrow for smaller river discharges, which causes more friction between the tide and the banks causing a lower salt intrusion. For some estuaries, the salt intrusion length increases for river discharges above the yearly averaged discharge, since friction diminishes. River-dominated estuaries, where the river discharge is much larger than the tidal discharge, experience much more narrowing. It becomes difficult for the tide to enter the estuary causing a large reduction in salt intrusion length on the long term. River discharge has a small influence on the salt intrusion length and morphology of tide-dominated systems. Mixed systems have a large increase in salt intrusion when the river discharge decreases on both the short and the long timescale, since widening of the estuary mouth causes that the tide can still easily enter after narrowing. This 1D numerical model can be used for further research when the goal is to gain insight into the long term evolution of estuaries, for example when the effects of sea-level rise or sediment deficits are investigated.

Contents

1	Introduction	5
1.1	Thesis outline	6
2	Theoretical background	7
2.1	Estuarine properties	7
2.2	Salt intrusion in estuaries	12
2.3	River discharge change	14
3	Research objective	16
4	Model & data description	18
4.1	1D numerical estuary model	18
4.2	Estuary data set	20
5	Methods	22
5.1	Testing the model hydrodynamics	22
5.2	Calibration of width prediction	22
5.3	Predictor for salt intrusion length	23
5.4	Changing the river discharge	25
6	Results	27
6.1	Calibration of width prediction	27
6.2	Testing the predictor for salt intrusion length	28
6.3	Salt intrusion length prediction	29
6.4	Width response to changing river discharge	30
6.5	Effect of changing river discharge on salt intrusion	31
7	Discussion	35
7.1	Estuarine hydrodynamics and morphology	35
7.2	Salt intrusion length and change in river flow	37
7.3	Future research	38
8	Conclusion	40
A	Notation	46
B	Estuary data	48
C	Testing the model hydrodynamics	50
D	Predictive equations of Gisen et al. (2015)	52
E	Additional figures for results	54
F	Results for salt intrusion length and β_B and β_L	55

List of Figures

1	Shapes and patterns for a selection of well-known rivers (Nienhuis et al., 2018).	6
2	Classification triangle illustrating the division of deltas into fluvial-dominated, wave-dominated and tide-dominated types, based on Galloway (1975) and Nienhuis et al. (2020), source of maps: Google Earth ©2022 TerraMetrics (used February 2022).	8
3	Side view of the coastal systems from river to sea (Buschman, 2011).	9
4	Typical morphology of a tide-dominated estuary, based on Scanes et al. (2017) who based it on Dalrymple et al. (1992).	9
5	Global distribution of semi-diurnal, diurnal and mixed tides (from Pidwirny (2006)).	10
6	Global variation in tidal range (Davies, 1964; Rosendahl Appelquist & Halsnæs, 2015)	10
7	Three types of longitudinal distribution of salinity: a) a stratified (or salt wedge) estuary, b) a partially mixed estuary, and c) a well-mixed estuary (Savenije, 2012).	13
8	Hypothesis for a decreasing river discharge, a) Initial estuary morphology and salt intrusion limit, b) Hydrologic (short term) response to a river discharge decrease, c) Morphologic (long term) response to a river discharge decrease. Based on Nienhuis et al. (2018).	16
9	Sketch of modelled estuary, based on Janssen (2022). Note that the sea level is taken as the reference level for the z-axis.	18
10	Estuary data set. In blue: Nienhuis et al. (2018), in red: Gisen et al. (2015).	21
11	Schedule of model and methods. In blue (5.1): validation of the hydrodynamics; in orange (5.2): calibration of width prediction by finding the best α and β ; in green (5.3): validation of salt intrusion length predictor by a) directly inserting the input data in the salt intrusion equations, b) by using the hydrodynamics of the 1D tide-averaged model, c) by using both the hydro- and morphodynamics of the 1D tide-averaged model; in black (5.4): changing the river discharge and a) calculate the hydrodynamics and its salt intrusion response and b) calculate the hydro- and morphodynamics and its salt intrusion response.	23
12	Convergence lengths by Gisen et al. (2015). Numbers and corresponding estuary names can be found in table 3 of appendix B.	25
13	Total RMSE for river width and mouth width combined, 1 to 3 indicates the top 3 lowest RMSE for the combinations of α and β	27
14	RMSE for width ratio B_m/B_r , 1 to 3 indicates the top 3 lowest RMSE for the best combinations of α and β	27
15	Best fits for the river width, mouth width and width ratio ($\alpha = 6$ and $\beta = 0.575$).	28
16	Calculated or modelled salt intrusion length against measured salt intrusion length. (a) Data from Gisen et al. (2015) directly in method of Savenije (1993), (b) Hydrodynamics from 1D tide-averaged model, morphology from Gisen et al. (2015), (c) Hydro- and morphodynamics from 1D tide-averaged model.	29
17	The salt intrusion length for the systems in the data sets of Nienhuis et al. (2018) and Gisen et al. (2015) against the tide dominance ratio.	29
18	Morphological response of the mouth width to changing river discharge, the river width response is given by the dotted line. When the slope of the line is close to 0.575, the estuary is river-dominated (delta), while a slope close to 0 means that the estuary is tide-dominated.	30
19	The power in the relation between $Q_{r,ratio}$ and $B_{m,ratio}$, the slope of the lines in figure 18. The closer β_B is to 0.575, the more river-dominated the estuary is.	30
20	Salt intrusion change in response to changing river discharge on the short term (no morphodynamic change). Every line represents an estuary.	31
21	Salt intrusion change in response to changing river discharge on the long term (hydro- and morphodynamic change). Every line represents an estuary.	31
22	Morphological response and salt intrusion on the short term and long term for a river-dominated, mixed and tide-dominated system. The dotted lines indicate the maximum salt intrusion length.	33
23	Relative salt intrusion length as function of river discharge ratio at the short term and long term.	34
24	Exponent β_L of the river discharge as power function for the salt intrusion length for the short and long term compared to river- and tide-dominance.	34
25	Trapezoidal width profile (Nienhuis et al., 2018).	51
26	Tidal prism comparison between the 1D tide-averaged model and the model by Nienhuis et al. (2018)	51

27	Tidal prism ratio against estuary length over tidal wavelength	51
28	RMSE for river width ratio $B_{r,mod}/B_{r,obs}$, 1 to 3 indicates the top 3 lowest RMSE for the combinations of α and β	54
29	RMSE for mouth width ratio $B_{m,mod}/B_{m,obs}$, 1 to 3 indicates the top 3 lowest RMSE for the combinations of α and β	54
30	Tidal excursion length, only hydrodynamics from 1D tide-averaged model.	54

List of Tables

1	Constant parameters used.	19
2	Symbols and units used in this report.	46
3	Estuary data by Nienhuis et al. (2018) and Gisen et al. (2015) used in this research. . . .	48
4	The tide-dominance ratio I and salt intrusion length L^{HWS} for the yearly averaged river discharge for all estuaries. The exponent β_B in the river discharge-width relation and the exponent β_L for the river discharge-salt intrusion relation on the short term and long term for the estuaries of the data set by Nienhuis et al. (2018).	55

1 Introduction

Estuaries are transitional zones between the river and open sea, where fresh and salt water can mix forming a brackish environment. Estuaries have a high societal, economical and environmental relevance and they belong to the most productive and dynamic systems in the world (Bolla Pittaluga et al., 2015; Boerema & Meire, 2017). The sheltered brackish waters provide a unique habitat attracting a high variety of animal and plant species, which results in a great biodiversity (Bolla Pittaluga et al., 2015). Coasts and estuaries have always been important to humans as well, both as a source of food and as a transport link between river and sea (Savenije, 2012). The adjacent floodplains contain very fertile soils, which makes deltaic regions centers of population and agriculture (Syvitski & Saito, 2007). Around 60% of the global population lives along the coasts and estuaries (Bianchi, 2013). Twenty-one of the world's thirty largest cities are built near estuaries including among others New York, Tokyo, Buenos Aires and London (Wolanski & Elliot, 2015; Leuven et al., 2019). At the same time, estuaries are very fragile environments due to their transitional character (Savenije, 2012). This raises questions about their fate in a century of overpopulation and global warming (Bolla Pittaluga et al., 2015).

Since estuaries occur between the river and sea, they have a dynamic transition between salt and fresh water depending on the fluvial and marine processes. Regions with salt or brackish water consist of very different ecological environments than regions with fresh water (Boerema & Meire, 2017). Salinization often brings negative ecological impacts, such as eutrophication of coastal wetlands and biodiversity reduction (Ardón et al., 2013; Cañedo-Argüelles et al., 2013; Noe et al., 2013). Furthermore, it may constrain the possibility of using water for irrigation and human consumption (Teh & Koh, 2016). For farmers, brackish irrigation or seepage water can affect their crop production and can lead to land degradation on the long term (Saysel & Barlas, 2001; Bless et al., 2018). Salt water might also infiltrate into fresh groundwater reservoirs close to the estuary, which can harm the drinking water supply (Teh & Koh, 2016). Due to the serious effects that salt water might have, it is important to know how far salt water intrudes within the estuary. This is called the salt intrusion length, which is the distance from the estuary mouth to the point where the salinity reaches the river salinity (Savenije, 1993).

The salinity intrusion into the river mouth is affected by the river discharge, which might change due to the seasons, climatic changes and anthropogenic drivers (Haddeland et al., 2014). Climate change leads to an increase in the frequency and extent of droughts, due to temperature increases and changes in precipitation regimes (Prudhomme et al., 2014). During the dryer dry seasons, the lower river discharge allows salt water to travel further upstream in the river. At the same time, the wet seasons will become wetter, causing that the increased river discharge pushes the salt intrusion further seawards. The seasonal fluxes occur at rather small timescales. On an annual basis, it depends on the geographical location whether an increase or decrease in yearly averaged river discharge will occur (van Vliet et al., 2013). Regarding the human activities, hydropower dams and increasing irrigation demands will cause changes in the river discharge regime (Savenije, 2012). Hydropower dams will dampen the extremes in dry and wet periods, having an opposite effect of climate change (Räsänen et al., 2017). When irrigation water is coming from the surface waters, river discharge might decrease, while irrigation water coming from groundwater might increase the river discharge (Gerten et al., 2008). Although it depends on the individual estuary whether the river discharge will actually change in an increasing or decreasing direction, it will be important to know the response of estuaries to river discharge in advance.

Several studies have been done to the effect of river discharge on salt intrusion, but most assume estuaries are in morphologic equilibrium whereby a morphostatic model can be used to simulate estuarine hydrodynamics (Savenije, 1993; Liu et al., 2007; Gong & Shen, 2011; Gisen et al., 2015). The estuarine morphology results from some typical forcing factors: river flow, tidal motion, wave action and sometimes also gravitational circulations driven by salinity and density gradients (Bolla Pittaluga et al., 2015). Figure 1 shows the large differences in delta and estuarine shapes. Many studies prescribe a convergent funnel-shaped width profile, meaning that the estuary has a larger width at the mouth than upstream (Savenije, 1993; Lanzoni & Seminara, 2002; Todeschini et al., 2008; Canestrelli et al., 2014; Bolla Pittaluga et al., 2015; Gisen et al., 2015). The channel banks are fixed regardless of the channel properties or boundary conditions. However, long term changes in estuarine conditions like the river discharge can upset the estuarine balance, which might induce morphological adjustment (Nienhuis et al., 2018). The estuary width and depth might change, which will in turn change the fluvial and tidal hydrodynamics and salt intrusion length. This indicates that a morphostatic model might not result in reliable predictions on the long term.

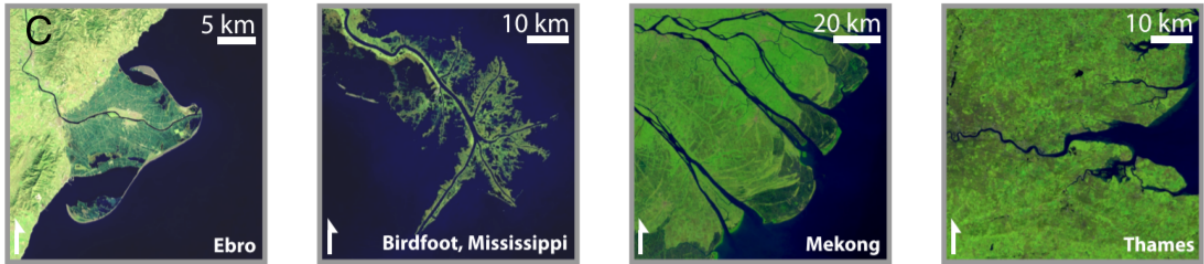


Figure 1: Shapes and patterns for a selection of well-known rivers (Nienhuis et al., 2018).

During this research, the effect of a changing river discharge on the salt intrusion length for morphodynamic estuaries will be studied. This is done by using an existing one-dimensional numerical hydrodynamic and morphodynamic model, where the width can adjust to the channel properties and boundary conditions (Iwantoro et al., 2021; Janssen, 2022). The width prediction of this theoretical model will be optimized by comparing it to existing data. This model will be expanded with a salt intrusion prediction by using some empirical relations based on Savenije (1993). We will study the salt intrusion length on the short term, where we assume there is no morphology change, and on the long term, where we assume there is a morphological change. Finally, we will try to find relations between the river discharge and salt intrusion length for river-dominated systems, tide-dominated systems and mixed systems.

1.1 Thesis outline

This thesis report consists of 8 chapters and an appendix section. A first insight into the subject is presented in the Introduction (section 1). Some theoretical background about estuarine properties, salt intrusion and river discharge changes is given in section 2. After that, the research questions, objectives and hypotheses are formulated in section 3. Section 4 includes a model description to explain the numerical model used in this research. A data description is also included in this section, explaining two data sets by Nienhuis et al. (2018) and Gisen et al. (2015) which will be used for testing, calibration and predictions. The methods are described in sections 5, in an order based on the research objectives. In section 6, the results will be presented and briefly discussed. A further discussion of the results and a comparison of the results to earlier research can be found in section 7, the discussion. Section 7 also contains some suggestions for future research. Finally, section 8 contains the conclusions of the research. In the appendices, the symbols and units used are given in appendix A, while appendix B contains the estuary data used in this research. Appendix C gives the methods and results for testing the hydrodynamics in the model and appendix D contains an extra section about predictive equations for the salt intrusion length. Appendices E and F give some additional figures and the final results in a tabular format.

2 Theoretical background

In this section, the estuarine properties are discussed at first to give a general overview of estuarine definitions and classification and the hydrodynamics and morphology. After that, salinity distributions, characteristics and formulas are explained. Lastly, the factors that change the river discharge and the effects of a changing river discharge are discussed.

2.1 Estuarine properties

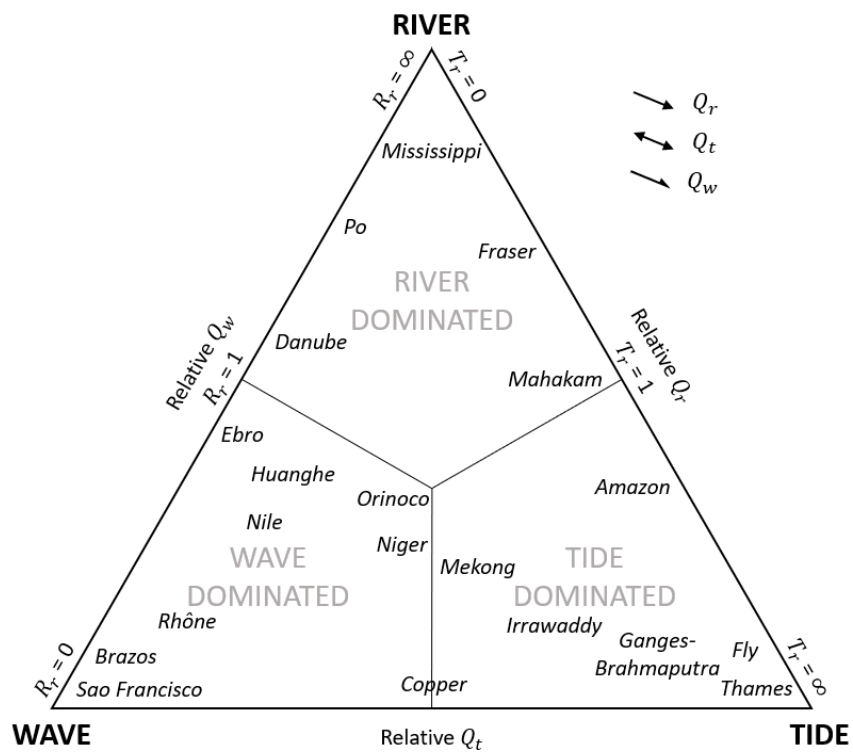
Over the past decades, many definitions and classifications of estuaries have been made (Pritchard, 1967; Hume & Herdendorf, 1988; Davidson et al., 1991; Dalrymple et al., 1992; Perillo, 1995). The definition and classification used depends on the nature of the research (Leuven et al., 2016). For example, the definition of an estuary will be different from a biological or geochemical viewpoint compared to a morphological viewpoint (Pritchard, 1967). Since the focus of this study will be on the morphology and salinity of estuaries, both the morphological and chemical aspects are important. A widely-used chemical definition of an estuary was given by Pritchard (1967), defining an estuary as the area of a river mouth where seawater and freshwater derived from land drainage are measurably diluted with a range from 0.1‰ till 30-35‰. This definition is useful for studying the chemical and biological processes in the fluvial-marine transition zone, but might be of limited use when dealing with physical and morphological processes (Dalrymple et al., 1992). When focusing on the dynamics, morphology and equilibrium of estuaries in combination with salinity, the following definition is better suitable for this thesis: An estuary is a partially enclosed water body with an open connection to the sea at the seaward boundary where salt water can enter by the penetration of tides and waves and a fresh river water inflow at the landward boundary causing that sea water is significantly diluted with fresh water (Perillo, 1995; Leuven et al., 2016).

Estuaries can be classified based on their shape, tidal influence, river influence, geology or salinity for example (Savenije, 2012). Dalrymple et al. (1992) developed a framework for the classification of estuaries based on the relative importance of physical processes and temporal changes. The physical processes include the influence of river outflow, waves and tidal currents, while the temporal forcing includes sea-level rise and sediment supply. This framework was made quantitative by Nienhuis et al. (2018) and Nienhuis et al. (2020). Nienhuis et al. (2018) defined a tide-dominance ratio based on a discharge ratio:

$$I = \frac{Q_{t,max}}{Q_r} \quad (1)$$

where Q_r is the mean annual fluvial discharge ($\text{m}^3 \text{s}^{-1}$) and $Q_{t,max}$ is the maximum tidal discharge amplitude ($\text{m}^3 \text{s}^{-1}$). When $I > 1$, the system is tide-dominated, while $I < 1$ means the system is river-dominated. At $I = 1$, the tidal discharge has the same order of magnitude as the fluvial discharge (Nienhuis et al., 2018). Nienhuis et al. (2020) developed a ternary diagram which compares the fluvial sediment supply to the tide- and wave-driven sediment fluxes near the river mouth. Figure 2a shows a ternary diagram based on Nienhuis et al. (2020). Two important sediment flux ratios were defined: the fluvial dominance ratio R_r and the tidal dominance ratio T_r related to the tide-dominance discharge ratio of equation 1. The fluvial dominance ratio is the ratio between the fluvial sediment supply and the wave-induced sediment flux ($Q_{s,r}/Q_{s,w}$), while the tidal dominance ratio is the ratio between the tidal sediment flux and the fluvial sediment supply ($Q_{s,t}/Q_{s,r}$). The sediment fluxes have the unit kg s^{-1} . The relative importance of the river, waves and tides determines whether a delta is river-dominated, wave-dominated or tide-dominated, see figure 2. As can be seen in the maps included in figure 2b-2g, the morphology largely depends on the interactions between river, waves and tides.

Figure 3 displays the coastal systems surrounding an estuary. Between the river and estuary, a tidal river generally occurs. A tidal river is the downstream section of a river where tides penetrate, but sea water does not intrude (Dronkers, n.d.). The relative influence of the river and tides determines the limit of subtidal water level variation and the tidal rise limit. The tidal rise limit is the farthest point upstream where a river is affected by the daily tidal fluctuations, whereas the limit of subtidal water level variation is the most upstream point where the water level varies over a 14 days timescale, following the spring-neap cycle (figure 3, Buschman (2011) and Davis Jr and Dalrymple (2011)). The flood limit indicates the most upstream point where the flow velocities still change direction during a tidal cycle (Buschman, 2011). The limit of tidal influence generally extends further landward than the limit of sea



(a) Classification triangle



(b) Danube



(c) Mississippi



(d) Mahakam



(e) Sao Francisco



(f) Copper



(g) Fly

Figure 2: Classification triangle illustrating the division of deltas into fluvial-dominated, wave-dominated and tide-dominated types, based on Galloway (1975) and Nienhuis et al. (2020), source of maps: Google Earth © 2022 TerraMetrics (used February 2022).

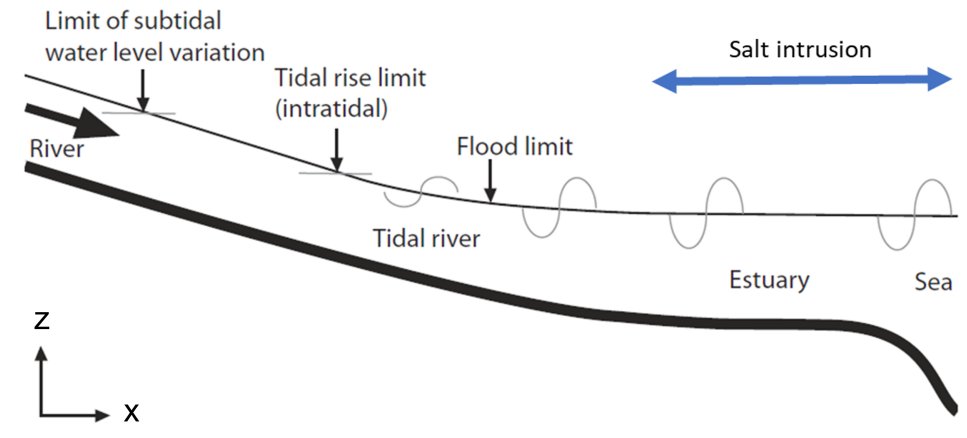


Figure 3: Side view of the coastal systems from river to sea (Buschman, 2011).

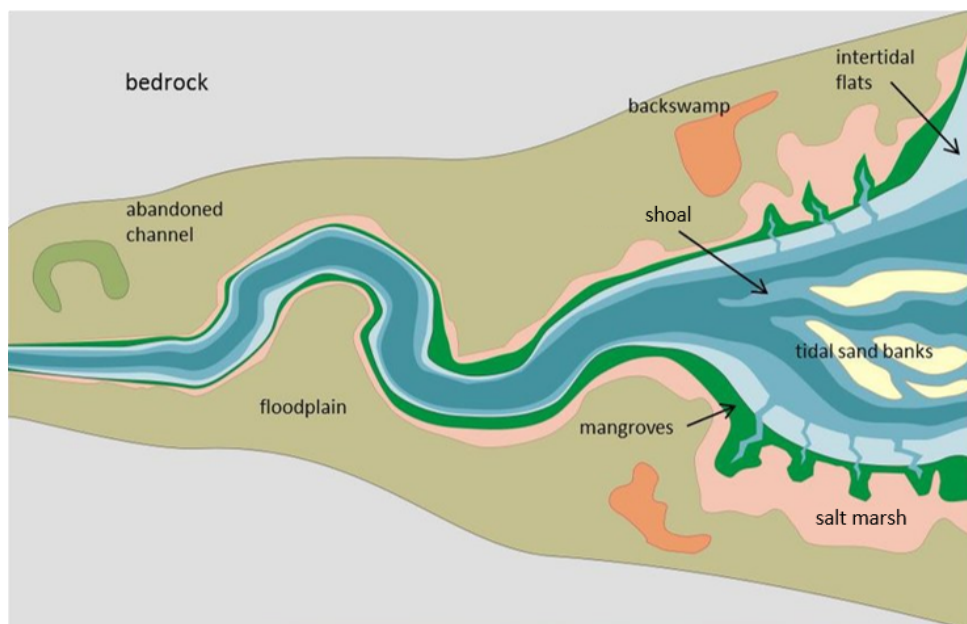


Figure 4: Typical morphology of a tide-dominated estuary, based on Scanes et al. (2017) who based it on Dalrymple et al. (1992).

water intrusion (Dalrymple et al., 1992). In an estuary, both tides and sea water intrudes. Often, an estuary does not directly mound into the open sea, but exchanges water with a tidal basin (Dronkers, n.d.).

Some properties, like the mean sea level, tidal wave propagation in the external sea basin and river flows in the surrounding catchment can be considered external to the estuary, meaning that they are independent of any system response (Townend, 2012). Those external forcings are determining the characteristic properties of an estuary, such as the mean tidal water level, tidal amplitude, tidal period and river discharge. The combination of forcings induces sediment transport by erosion and deposition. If the forcing conditions change, the erosion and deposition processes will change and the estuary adapts its geometry (Townend, 2012). In the absence of waves, the morphology is determined by the interaction between river discharge and tidal flows. River-dominance leads to an approximately constant width over the whole channel, see the Mississippi in figure 1 and 2c (Nienhuis et al., 2020). On the contrary, tide-dominated alluvial estuaries such as the Thames and Fly in figures 1 and 2g respectively, generally show a seaward widening of the channel banks, which is called convergence (Nienhuis et al., 2020). The river itself still has an approximately straight channel. The typical morphology of a tide-dominated estuary includes channels, shoals, intertidal flats and salt marshes, see figure 4.

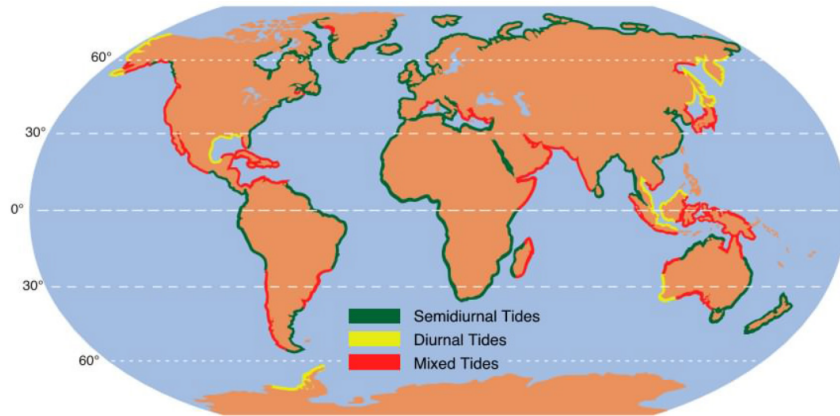


Figure 5: Global distribution of semi-diurnal, diurnal and mixed tides (from Pidwirny (2006)).

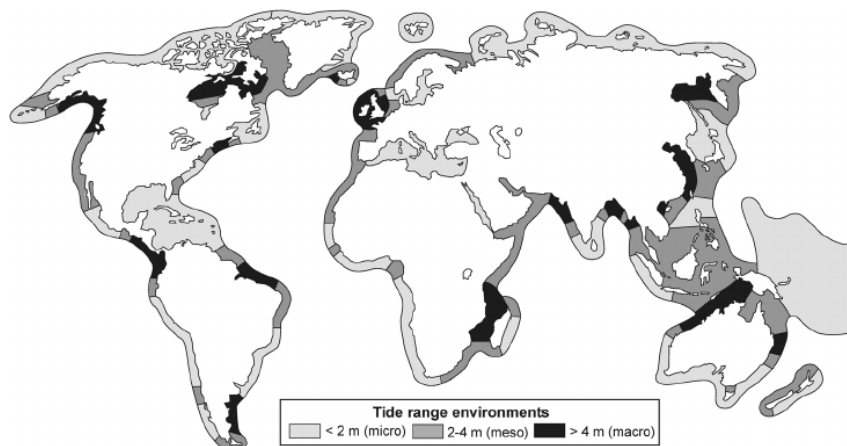


Figure 6: Global variation in tidal range (Davies, 1964; Rosendahl Appelquist & Halsnæs, 2015)

The two main tidal features are the tidal range and tidal period. The tidal range is measured as the height difference between the high water level and low water level, whereas the tidal period is the time between one high (or low) level and the next low (or high) level (Pugh & Woodworth, 2014). The two dominant types of tides are the semi-diurnal and diurnal tides, meaning that each tidal cycle takes roughly half a day or one day respectively. A map indicating the distribution of semi-diurnal, diurnal and mixed tides (both semi-diurnal and diurnal tides) globally is given in figure 5. Davies (1964) made a classification based on tidal range, where coastal environments are called micro tidal when the tidal range is smaller than two meters (<2 m), meso tidal when the tidal range is between two to four meters (2 – 4 m) and macro tidal when the tidal range is larger than four meters (>4 m). A map of tidal range environments is given in figure 6. With the rising and falling of the tide, a horizontal movement of water occurs, which is called the tidal current. The incoming tidal current into estuaries or bays along the coast is called the flood current, while the outgoing tidal current is called the ebb current. The strongest currents occur around the time of mean water level, while the weakest currents occur during high water or low water, also called the slack water. So, the tide is responsible for the harmonic pumping of water into and out of the estuary system.

The tidal hydrodynamics within an estuary are greatly influenced by the convergent shape and friction with the bed and banks (Friedrichs & Aubrey, 1994; Davies & Woodroffe, 2010). As the banks converge, the energy of the incoming tidal wave per unit width increases, meaning that the tidal amplitude is amplified (Savenije, 2001). At the same time, friction with the bed and banks causes an energy loss, meaning that the tide dampens (Davies & Woodroffe, 2010). This friction will become larger with decreasing water depth (Davis Jr & Dalrymple, 2011). In an ideal estuary, the amplification by width convergence is exactly compensated by the friction loss, so that there is no tidal amplification or damping throughout the estuary (Savenije, 2001). If the width and depth are constant over the length of the estuary and there is a tidal influence, the tidal velocities will increase towards the mouth of the estuary. This

leads to erosion at the downstream end of the estuary and results in the convergent shape (Davies & Woodroffe, 2010; Savenije, 2012). Furthermore, the tidal prism increases towards the mouth (Dronkers, 2017). The tidal prism is the volume of water that flows into the estuary during flood and leaves it during ebb (Sassi et al., 2012). This means that more water has to go through the estuary mouth than through the upstream part causing larger velocities and more erosion leading to convergence.

An estuary is in morphologic equilibrium when the forces that cause sediment transport within the system cancel each other out (Zhou et al., 2017). This leads to specific conditions of the system mass balance where there is no net sediment accumulation or erosion. Two different states of morphologic equilibrium are defined: morphostatic equilibrium and morphodynamic equilibrium. A morphostatic equilibrium means that there is no net sediment transport causing that the system is in balance and the morphology will not change. For a morphodynamic equilibrium, there might be a net sediment transport at a short time scale, but these small-scale changes will become subsumed in the longer term patterns of change (Zhou et al., 2017). When the time scale of the net sediment transport becomes longer, the estuary might develop towards a new morphodynamic equilibrium. However, there will always be a time lag between a change in the boundary conditions and the morphological adjustment (Zhou et al., 2017). A morphostatic modelling approach might be relevant for analyzing sediment dynamics at time scales of months or a few years, when the morphological changes remain relatively small compared to the hydrodynamic processes (Grasso et al., 2021). At longer time scales of decades to centuries, changes in the boundary conditions might result in a morphological change of the estuary, meaning that a morphodynamic approach is better suitable.

The width convergence of tide-dominated estuaries has been the subject of many previous studies, although the width was often kept constant over time meaning that the channel banks cannot erode or accrete (Lanzoni & Seminara, 2002; Todeschini et al., 2008; Canestrelli et al., 2014; Bolla Pittaluga et al., 2015). A very common expression for an ideal converging funnel-shaped estuary width can be described by the channel width B (m) following an exponential function:

$$B(x) = B_m \exp\left(-\frac{x}{L_b}\right) \quad (2)$$

with B_m is the width at the mouth of the estuary (m) and L_b is the width convergence length or e-folding length scale (m) defined as the distance from the mouth to the point where the width is reduced by a factor e (≈ 2.72 , Leuven et al. (2021)). x is the spatial axis, where $x = 0$ at the estuary mouth. For tide-dominated estuaries with a large convergence, L_b will become small and a large difference in width along the estuary occurs. Although equation 2 is developed for tide-dominated estuaries, it might also work for river-dominated systems, since L_b will become infinitely large, meaning that equation 2 becomes $B = B_m$ representing a straight channel (Savenije, 2012). A disadvantage of this equation is that the mouth width B_m needs to be known in advance, as well as the width convergence length L_b , which makes it difficult to use this equation for width predictions.

Nienhuis et al. (2018) described the convergent shape of tide-dominated estuaries as a trapezoidal width profile to predict the magnitude of downstream channel widening. They showed that the downstream channel widening can be quantified by the ratio of the tide-driven discharge and fluvial discharge in combination with a non-dimensional flow velocity scale:

$$B_m = \left(\frac{I}{U} + 1\right)B_r \quad (3)$$

where I is the tide-dominance ratio (-), B_r is the river width (m) and U is a non-dimensional velocity scale (-) which quantifies the strength of the tidal flow relative to the fluvial flow. Although this method seemed to work successfully, it is a large simplification to assume estuaries have a trapezoidal shape.

Miori et al. (2006) and Kleinhans et al. (2011) included a time-dependent width adaptation in their numerical hydro- and morphodynamic models for rivers based on an equilibrium width. They assumed that the width evolves towards an equilibrium width based on an empirical hydraulic geometry relation:

$$\frac{\partial B}{\partial t} = \frac{B_e - B}{T_w} \quad (4)$$

with B_e is the equilibrium width that the channel width evolves towards and T_w is a timescale on which this width adjustment happens. Kleinhans et al. (2011) and Janssen (2022) showed that this timescale T_w did not have an influence on the eventually reached equilibrium width, but only on how fast this equilibrium was reached. Both studies used an empirical hydraulic geometry relation between the equilibrium width of the river and the river discharge. Kleinhans et al. (2011) used a relation of the form:

$$B_e = aQ_r^b \quad (5)$$

To calculate the equilibrium width of tide-influenced estuaries, the tidal influence was incorporated in this equation by Janssen (2022). Sassi et al. (2012) developed a downstream hydraulic geometry relation for the cross-sectional area A (m) of a tidally influenced delta:

$$A = \alpha_A(Q_r + Q_{t,max})^{\beta_A} \quad (6)$$

where α_A and β_A are two empirical coefficients, Q_r ($\text{m}^3 \text{s}^{-1}$) is the river discharge and $Q_{t,max}$ ($\text{m}^3 \text{s}^{-1}$) is the maximum tidal discharge amplitude which is associated with the tidal prism (Sassi et al., 2012). Janssen (2022) rewrote this equation to a like wise power-law relation for the width:

$$B_e = \alpha(Q_r + Q_{t,max})^\beta \quad (7)$$

Janssen (2022) showed that this equation in combination with equation 4 of Kleinhans et al. (2011) developed a width profile that reaches an equilibrium. As default settings, Janssen (2022) used an α of 4 and β of 0.5, since most rivers correspond to this (Leopold & Maddock, 1953; Hey & Thorne, 1986; Xu et al., 2021). It was stated that β has the most effect on the width ratio B_m/B_r and width convergence length, meaning that the used value for β is very important for the width prediction (Janssen, 2022). Since estuaries show more convergence than rivers, some other studies found values for β around 0.70 for tide-influenced estuaries (Langbein, 1963; Myrick & Leopold, 1963; Rinaldo et al., 1999; Leuven et al., 2018). The study of Janssen (2022) only focused on theoretical relations between parameters without testing the equations on existing estuaries. More research should be done to the optimization of these parameters, since they are crucial in predicting the width profile.

2.2 Salt intrusion in estuaries

Following Herbert et al. (2015), salt water intrusion is the upstream movement of brackish or saline water in the river that causes concentrations of salt ions to increase above natural background levels. The salinity of sea water is about 35‰, while the salinity of river water is close to 0‰. Since estuarine water is a mixture, salinities are typically between 0.1‰ and 35‰, see section 2.1 (Pritchard, 1967). The tidal limit generally extends further into the river than the salt sea water intrusion (figure 3, Dalrymple et al. (1992)). For most estuaries, the salinity decreases from the seaward side to the landward side due to the freshwater input of the river (Geyer, 2010). However, the salinity can also increase in the landward direction due to excess evaporation in the upstream part, this is called an inverse estuary. Inverse estuaries only occur in arid climates where evaporation greatly exceeds the inflow of freshwater (Geyer, 2010).

When excluding inverse estuaries, generally three types of salt intrusion mechanisms can be found: 1) the stratified type, also called salt wedge type, 2) the partially mixed type, and 3) the well-mixed type (Savenije, 2012). Figure 7 illustrates the three types of salinity distributions. A salinity distribution of the stratified type occurs during high river discharges. Due to the higher density of salt water compared to fresh water and the energy that is available in the river discharge, a sharp interface between the salt water and fresh water occurs with a salt wedge beneath the fresh river water (Savenije, 2012). When the fresh water discharge is small compared to the tidal discharge, a well-mixed estuary can occur. For a stratified estuary, the vertical salinity gradient shows a sudden increase, a smooth vertical gradient can be found for a partially mixed estuary and no vertical gradient will be found in a well-mixed estuary. Following Uncles and Stephens (1996), an estuary can go through different stages of salinity distribution during a spring-neap cycle. During spring tide, the tidal discharge is large compared to the fluvial discharge meaning that a well-mixed salinity distribution will develop. During neap tide, the tidal amplitude and therefore tidal discharge are smaller and the relative influence of the river becomes larger, resulting in

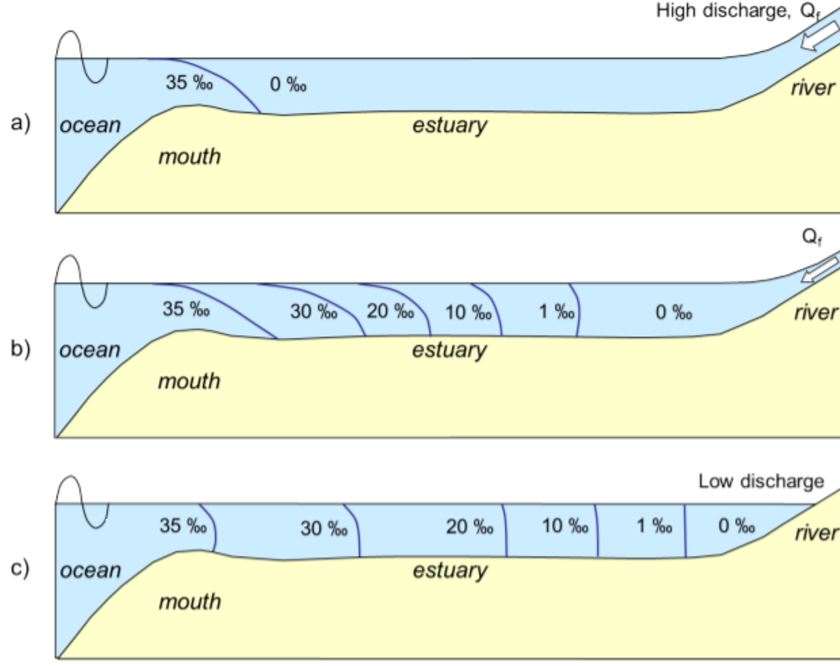


Figure 7: Three types of longitudinal distribution of salinity: a) a stratified (or salt wedge) estuary, b) a partially mixed estuary, and c) a well-mixed estuary (Savenije, 2012).

a stratified salinity distribution (Uncles & Stephens, 1996). In between spring tide and neap tide, a partially mixed salinity distribution will occur. In the Madaomen river, which is one of the distributary channels of the Pearl river, Gong and Shen (2011) found that the fluctuations of salt intrusion during a tidal cycle were minor, while a great fluctuation in salt intrusion was found during a spring-neap cycle. Also in this river, it was found that the estuary was more mixed at spring tide compared to neap tide. The maximum intrusion happened during the transition from neap to spring tide, usually 2-3 days after neap tides, while minimum intrusion occurred during the transition period between spring tide and neap tide, generally 3-5 days after spring tide. They also found a monthly variability in salt intrusion, whereby the strongest intrusion occurred before the secondary spring tides within a month (Gong & Shen, 2011).

To give a value to the saltwater intrusion, multiple numerical and empirical models have been developed for the prediction of the salt intrusion length (Savenije, 1993; MacCready & Geyer, 2010; Etemad-Shahidi et al., 2011; Gong & Shen, 2011; Cai et al., 2015; Gisen et al., 2015). The salinity intrusion length is the distance from the estuary mouth to the point where the salinity reaches the river salinity (Savenije, 1993). The salt intrusion length varies periodically during a tidal cycle. The maximum and minimum salt intrusion lengths during a tidal cycle occur at high water slack (L^{HWS}) and low water slack (L^{LWS}), respectively. The difference between L^{HWS} and L^{LWS} is called the tidal excursion length E , which is defined as the net horizontal distance travelled by a water particle from HWS to LWS or vice versa (Parsa & Etemad-Shahidi, 2010). The tidal average intrusion length (L^{TA}) is the average between the salt intrusion lengths at HWS and LWS (Savenije, 1989).

Savenije (1993) developed a relatively simple expression for the salt intrusion length at high water slack L^{HWS} (m):

$$L^{HWS} = L_a \ln \left(\frac{1}{\beta_m} + 1 \right) \quad (8)$$

where L_a is the cross-sectional area convergence length (m) and β_m is a positive coefficient which determines the longitudinal variation of dispersion. Since β_m is a positive number, the argument of the natural logarithm is always larger than unity. β_m can be calculated by

$$\beta_m = \frac{KL_a}{\alpha_m A_m} \quad (9)$$

with K is the Van der Burgh's coefficient, which is a sort of shape factor influencing the shape of the salt intrusion curve (figure 7, Savenije (1989)), α_m is the mixing coefficient at the estuary mouth and A_m is the cross-sectional area at the estuary mouth (m^2). Via an empirical analysis, Savenije (1993) determined empirical equations relating K and α_m to quantifiable estuary numbers. Each estuary has its own characteristic value for the Van der Burgh's coefficient K (Savenije, 1989). Following Savenije (1993), these dimensionless ratios appeared to correlate well with K :

$$\Pi_1 = \frac{h_m}{L_b} \quad (10) \quad \Pi_2 = \frac{H_m}{h_m} \quad (11) \quad \Pi_3 = \frac{h_m}{B_m} \quad (12) \quad \Pi_4 = \frac{T\sqrt{gh_m}}{H_m} \quad (13)$$

where h_m and H_m are respectively the channel depth (m) and tidal range (m) at the estuary mouth and L_b is the width convergence length (m). When Savenije (1993) combined equations 10-13 in a regression analysis, the following empirical relation was found:

$$K = 0.16 \times 10^{-6} \Pi_1^{1.10} \Pi_2^{1.66} \Pi_3^{0.13} \Pi_4^{2.24} (0 < K < 1) \quad (14)$$

After substituting the ratios Π_i , Savenije (1993) found that the resulting formula reads as:

$$K = 0.16 \times 10^{-6} \frac{h_m^{0.69} g^{1.12} T^{2.24}}{H_m^{0.59} L_b^{1.10} B_m^{0.13}} \quad (15)$$

The mixing coefficient at the estuary mouth α_m in equation 9 is calculated by:

$$\alpha_m = 220 \frac{h_m}{L_a} \sqrt{\frac{E_m T g h_m}{-Q_r A_m}} \quad (16)$$

with E_m is the tidal excursion length at the mouth (m).

Etemad-Shahidi et al. (2011) compared different salinity intrusion length approaches and concluded that the model of Savenije (1993) outperforms the others. However, Savenije (1993) used a width equation similar to equation 2 and kept it constant over time. As stated in section 2.1, the width profile of estuaries is morphodynamic and can change when boundary conditions change. No analytical or numerical model has been developed yet that calculates the salt intrusion length under changing width conditions and it will be good to do more research into this.

Furthermore, many studies showed that the salt intrusion length generally follows a power law relationship to river discharge: $L_s \propto Q_r^n$, where the power n varies in a wide range under different estuarine conditions (Abood, 1974; Monismith et al., 2002; MacCready & Geyer, 2010; Gong & Shen, 2011). Values found for n vary between $-1/7$ for low river flow conditions and -1 for high river flow conditions (Abood, 1974; Monismith et al., 2002). Again, those studies assumed the estuary width will not change, although a persistent change in river discharge will definitely affect the morphology of the estuary on the long term. This morphology change will in turn affect the salinity intrusion.

2.3 River discharge change

River discharge can be seen as an external forcing to the estuary, since it is independent of the estuary response (Townend, 2012). Where the sea primarily stores water, a river transports and does not retain water (Savenije, 2012). A river has more or less parallel banks and the bottom slope defines the direction of flow. At the upstream part of the estuary, the (tidal) river enters and brings in fresh water, nutrients and riverine sediments. River flow is always present, but the amount of river discharge is time-dependent. Many river areas experience wet and dry periods over the year associated with the wet and dry seasons. As already mentioned in the Introduction, due to climate change, wet seasons might become wetter resulting in larger wet season river discharge, while dry seasons might become dryer resulting in lower dry season river discharge meaning that climate change amplifies the extremes (van Vliet et al., 2013). Yearly averaged river discharge increases in the high northern latitudes due to increased precipitation with an earlier start of the snowmelt peak, and in the tropical zones due to increases in monsoon rainfall

(Nohara et al., 2006; van Vliet et al., 2013). A yearly averaged decrease in river flow was found in the mid northern latitudes and the southern latitudes. The temperature change associated with climate change will affect the evapotranspiration, snow/glacier melt in the mountains and vegetation cover, which will in turn affect the water discharges towards and in the river (Yang et al., 2015).

The construction of dams could have exactly the opposite effect regarding the seasonality of river discharge. Hydropower dams are built to improve the regional energy supply and sometimes to increase flood safety (Räsänen et al., 2017). The dams have large impacts on the downstream discharge regime. Directly after construction, the river discharge might drastically decrease, since water will be trapped behind the dam. During the wet season the reservoirs behind the dams will fill up with water meaning that the wet season discharge will decrease. In the dry season, the hydropower operations will lead to an increased dry season discharge, since more water is coming from the reservoir through the dam than that would normally go through the river (Räsänen et al., 2017; Eslami et al., 2019). In a tide-dominated estuary under natural conditions, sediment is exported out of the estuary during high river discharges, while sediment is imported into the estuary under low river discharges (Hoitink et al., 2017). When the flood events become more rare because of the dam, the increase in periods of tidally driven sediment import will lead to estuary infilling (Nienhuis et al., 2018).

The increase in global population leads to an increase in agricultural consumption including the necessity of irrigation. If the amount of irrigation is regionally significant, it can affect the river discharge (Gerten et al., 2008). As was also stated in the Introduction, irrigation can have two different and opposing effects. When the irrigation water is tapped from surface waters, it might decrease the river discharge, since a lot more water will evaporate and part of the water is taken up by the crops. However, the river discharge can also increase when the irrigation water is coming from fossil groundwater. Part of this water will enter the river system and thus increases the discharge compared to non-irrigated conditions (Gerten et al., 2008).

Many large rivers in the world have experienced declines in fresh water flows due to extraction and regulation (Herbert et al., 2015). Yang et al. (2015) found that in the Yangtze river, the mean annual river discharge of the first decade after closure of the Three Gorges Dam was about 7% lower than that of the 50 years before closure. About 60 to 70% of this decline was attributed to decreased precipitation, while the remainder was a result of the construction of the reservoirs, improved water-soil conservation and increased water consumption (Yang et al., 2015). Also in the Yellow river, Nile, Orange, Fraser and Columbia river, the river runoff shows a decreasing trend (Shi et al., 2019). Reasons for the reduction in river discharge in those rivers include both climate change and human activities such as excessive water abstraction for irrigation and industrial use. On the contrary, upward trends in mean annual river discharge were found for the Mississippi and Orinoco rivers from 1960 to 2010. Shi et al. (2019) found that the river discharges of the 40 largest global rivers directed towards the oceans show downward trends for 23 rivers, while upward trends were found for 17 rivers. Furthermore, climatic factors were the main influencing factors for these river discharge trends, and about 25% of the rivers was greatly affected by human activities (Shi et al., 2019).

Many factors can influence the river discharge and the occurrence or amount of increasing or decreasing river discharge depends on the individual estuary. River discharge change will affect the salt intrusion length, which might have large consequences for the estuary and estuary's surroundings (Monismith et al., 2002; Gong & Shen, 2011). For example, in the Pearl river, the salt intrusion length has increased in recent years due to decreased river discharges which resulted in a threatening of the fresh water supply in the surrounding regions (Gong & Shen, 2011). Therefore, it is important to research the salt intrusion and width response of rivers to changes in upstream discharge conditions.

3 Research objective

The theoretical background (section 2) indicates that there is no clear quantitative theory on how salt intrusion develops with respect to the river discharge when the estuary width can freely adapt. Previous research has been done to the effect of river discharge on salt intrusion, but those studies assumed estuaries are in morphostatic equilibrium (Savenije, 1993; Liu et al., 2007; Gong & Shen, 2011; Gisen et al., 2015). Furthermore, the morphodynamic equilibrium of rivers and estuaries has been extensively researched (Lanzoni & Seminara, 2002; Miori et al., 2006; Kleinhans et al., 2011; Sassi et al., 2012; Braat et al., 2017; Zhou et al., 2017; Janssen, 2022). This thesis will study the effects of changing river discharge on the salt intrusion length on the short term (constant width) and long term (changing width) in estuaries globally by using a one-dimensional hydrodynamic and morphodynamic model (Iwantoro et al., 2021; Janssen, 2022). On the long term, a time-variable channel width is included based on the river model of Miori et al. (2006) and Kleinhans et al. (2011), which was implemented in the one-dimensional model by Janssen (2022). A prediction of the salt intrusion length is added to the one-dimensional model based on the model of Savenije (1993).

The main research question is:

What is the salt intrusion response of morphodynamic estuaries to changing river discharge?

As discussed in section 2.1, the morphology or width profile changes on a much longer timescale than the hydrodynamics (Zhou et al., 2017; Grasso et al., 2021). This leads to the expectation of an approximately constant width on a short timescale of months to some years and a changing width on a longer timescale of decades to centuries. As was also discussed in section 2.1, river-dominated systems and tide-dominated systems have very different morphologies, indicating that the salt intrusion behaviour might also be different. This led to the following sub-questions:

- What is the width response of estuaries to changing river discharge?
- What are the differences in salt intrusion response on the short term and long term?
- What are the differences in width and salt intrusion response between river-dominated systems and tide-dominated systems?

The underlying hypothesis for a decrease in river discharge is displayed in figure 8. Decreasing river discharge is initially expected to lead to an upstream movement of the salt intrusion limit on the moment that the morphology has not yet adapted (Savenije, 2012). Since the width is still wide, the river flow velocities will decrease meaning that the tide is less damped by friction between the river flow and incoming tide (Braat et al., 2017). On the long term, it is expected that the river discharge decrease will lead to narrowing of the estuary, which might reduce the salt intrusion length (Savenije, 2012; Nienhuis et al., 2018). It will depend on the relative amounts of decrease in river discharge and narrowing whether the salt intrusion length still increased with respect to the initial salt intrusion length. A river discharge increase is expected to lead to the opposite result. Then, it is hypothesized that there is a decrease in salt intrusion length on the short term, while the estuary will become wider on the long term leading to

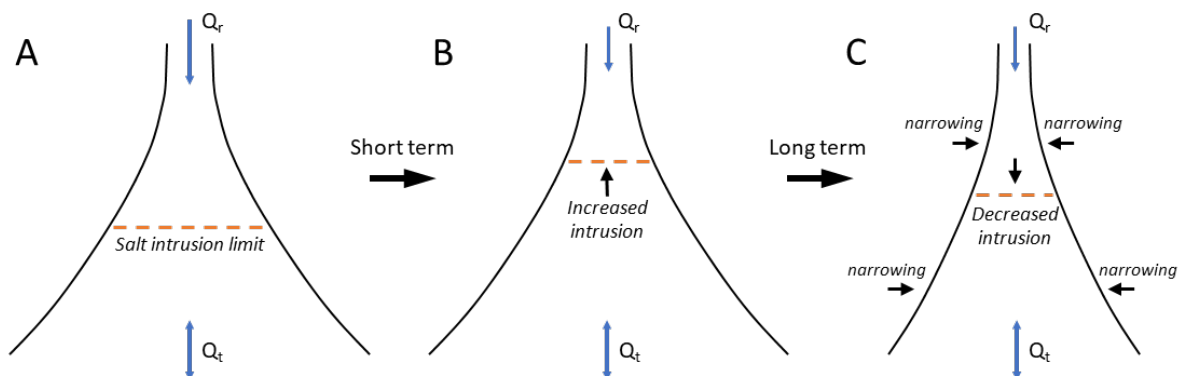


Figure 8: Hypothesis for a decreasing river discharge, a) Initial estuary morphology and salt intrusion limit, b) Hydrologic (short term) response to a river discharge decrease, c) Morphologic (long term) response to a river discharge decrease. Based on Nienhuis et al. (2018).

a relative increase in salt intrusion. For river-dominated systems, these effects are expected to be larger than for tide-dominated systems, since the hydrodynamics and morphology of the system will be more influenced by the river discharge.

To answer the questions, a model-based approach is used following 5 steps: 1) Testing the model hydrodynamics by comparing it to existing data; 2) Improvement of the morphologic width prediction by calibrating the model with existing data; 3) Adding and testing a predictor for the salt intrusion length; 4) Determine the morphological response of estuaries to changing river discharge; 5) Translate changing river discharge and the estuary's morphological response to salt intrusion.

4 Model & data description

To study the salt intrusion change in estuaries as a result of river discharge changes, a numerical model and two data sets are used. The hydrodynamic and morphodynamic calculations are based on an existing theoretical model and will be discussed and explained in section 4.1. The width prediction is optimized by using a data set by Nienhuis et al. (2018), while the method for the salt intrusion length of Savenije (1993) is tested by comparing it to data of Gisen et al. (2015). The data sets of Nienhuis et al. (2018) and Gisen et al. (2015) will be explained in section 4.2.

4.1 1D numerical estuary model

To simulate the hydrodynamic and morphodynamic response of estuaries, a one-dimensional (1D) numerical tide-averaged estuary model is used, based on Iwantoro et al. (2021). Initially, this model was used to simulate the hydro- and morphodynamics of bifurcating river channels. However, to get a better understanding of width and depth adjustment processes, the model was simplified to simulate only one channel without bifurcations (Janssen, 2022). Furthermore, equations were added to include dynamic width and depth predictions (Janssen, 2022). During this research, we are interested in the width prediction, while the bed level is kept constant.

The hydrodynamics are computed by numerically solving the Saint-Venant equations:

$$B \frac{\partial Z}{\partial t} + \frac{\partial Q}{\partial x} = 0 \quad (17)$$

$$\frac{\partial Q}{\partial t} + \frac{\partial}{\partial x} \left(\frac{Q^2}{A} \right) + gA \frac{\partial Z}{\partial x} + C_d \frac{|Q|QW_p}{A^2} = 0 \quad (18)$$

where x and t are the spatial and temporal axes, B is the channel width (m), Z is the water level (m), Q is the discharge ($\text{m}^3 \text{s}^{-1}$), A is the cross-sectional area of the channel (m), g is the gravitational acceleration ($= 9.81 \text{ m s}^{-2}$), C_d is the drag coefficient (-) and W_p is the wetted perimeter of the channel (m). The assumption is made that the channel has a rectangular cross-section where $A = Bh$ and $W_p = B + 2h$ with h is the channel depth (m). Figure 9 displays a sketch of the modelled estuary shape with some of the estuary properties. The Saint-Venant equations include the mass and momentum balances and are solved by using an implicit Preissmann scheme, for more details see Cunge et al. (1980) and Iwantoro et al. (2021).

The model consists of two types of nodes: the open boundary nodes at the upstream end and downstream end and the nodes in between the open boundary nodes. At the upstream boundary node, a river discharge condition can be applied by adding a self-defined discharge, by imposing an equilibrium discharge based on Bolla Pittaluga et al. (2015) or by using an empirical relation between width and discharge. Since

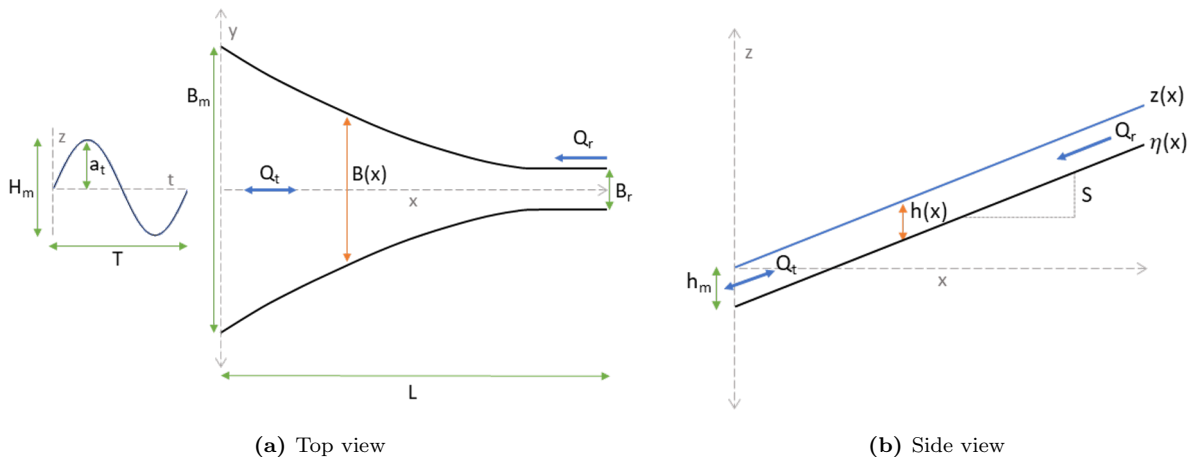


Figure 9: Sketch of modelled estuary, based on Janssen (2022). Note that the sea level is taken as the reference level for the z -axis.

Table 1: Constant parameters used.

Parameter	Value
Gravitational acceleration g	9.81 m s^{-2}
Drag coefficient C_d	2.725×10^{-3}
Spatial step Δx	$L_e/100 \text{ m}$
Time step Δt	300 s
Timescale for width change T_w	5 days

we are interested in the effect of river discharge on the width, we use a self-defined discharge and let the width depend on this via an empirical hydraulic geometry relation.

To include a morphodynamic width prediction, the time-dependent width adaptation by Miori et al. (2006) and Kleinhans et al. (2011) was implemented into the 1D numerical model by Janssen (2022):

$$\frac{\partial B}{\partial t} = \frac{B_e - B}{T_w} \quad (19)$$

where the equilibrium width B_e (m) depends on the river discharge and tidal discharge based on this hydraulic geometry formula:

$$B_e = \alpha(Q_r + Q_{t,max})^\beta \quad (20)$$

where α and β are two empirical coefficients, Q_r ($\text{m}^3 \text{ s}^{-1}$) is the river discharge and $Q_{t,max}$ ($\text{m}^3 \text{ s}^{-1}$) is the maximum tidal discharge amplitude (Sassi et al., 2012; Janssen, 2022). Since there is no tidal influence far upstream in the river, the tidal discharge amplitude $Q_{t,max}$ at the most upstream node becomes zero. It is assumed that the river at the upstream boundary is in equilibrium, therefore the empirical relation (equation 20) for the equilibrium river width (B_r) becomes

$$B_r = \alpha Q_r^\beta \quad (21)$$

At the downstream boundary node, a water level is prescribed including a tidal influence. In the case of one tidal constituent, the formula for the water level at the mouth Z_m (m) reads as

$$Z_m = a_t \sin\left(\frac{2\pi}{T}t - \phi\right) \quad (22)$$

where a_t , T and ϕ are the tidal amplitude (m), tidal period (s) and tidal phase (rad) at the mouth respectively. We used one tidal constituent, which is a diurnal or semi-diurnal tide depending on the estuary.

The bed elevation η (m) is taken constant over time and calculated by:

$$\eta = -h_m + Sx \quad (23)$$

with h_m is the channel depth at the mouth (m) and S is the channel slope (-).

The spatial step Δx is defined as the estuary length divided by 100 to make sure every estuary has the same number of nodes (101 nodes). The relatively small number of nodes limits the calculation time. The simulation time was set to 120 days, since it seemed that this was enough to reach a morphologic equilibrium. The time step Δt was set to 300 s, although the results were only stored for every 12 h, so for every tidal cycle of semi-diurnal tides. The width adaptation started after 5 days to let the hydrodynamics become stable at first. The timescale for width adjustment T_w is also set to 5 days, see table 1. This thesis was based on a modelling study using the modelling environment Matlab[®].

4.2 Estuary data set

The one-dimensional estuary model has to be tested and calibrated by comparing outputs to observed data to make sure the model is suitable for real estuary predictions. The observed data is obtained from two different data sets of Nienhuis et al. (2018) and Gisen et al. (2015) and completed with Google Earth data. The data of both data sets is displayed in table 3 in appendix B.

Data by Nienhuis et al. (2018)

The data set by Nienhuis et al. (2018) consists of data for 72 river systems worldwide ranging from very river-dominated systems to very tide-dominated systems with tide-dominance ratios I varying between the order of 10^{-3} and 10^3 . It contains measured yearly-averaged data about the river discharge, tidal range and period and about the estuary's shape, like the depth, slope, width and length. The tidal and fluvial characteristics were obtained from data by Syvitski and Saito (2007) and supplemented by WBMSed (Cohen et al., 2013) and TOPEX (Egbert & Erofeeva, 2002).

The river channel width was measured by Nienhuis et al. (2018) as the width upstream of the distributary network (if present) where the width becomes roughly constant. The mouth width was measured at the most downstream location where the width still increases gradually and the banks are self-formed, although this might be ambiguous, see the supplement of Nienhuis et al. (2018). For systems with multiple distributary channels, the summed width of the multiple channels is greater than the upstream channel width even without tides. To correct for this, and to focus on the effect of tides on one-channel systems, the single distributary channel width is estimated as the sum of all distributary channel widths multiplied by $n^{-0.5}$, such that $B_m = n^{-0.5} \sum_{i=1}^n B_i$, where n is the number of distributary channels.

The upstream channel depth h_r followed from hydraulic geometry rules based on the mean annual discharge (Mikhailov, 1970). For the delta channel slope measurements, SRTM data was used (Farr et al., 2007). For every system, the channel was followed from 0 to 10 meters above mean sea level to obtain a robust profile (Nienhuis et al., 2018). They fitted a second-degree polynomial function through the elevation data and retrieved the slope S of the fitted function at the channel mouth. The estuary length is then calculated as $L_e = h_r/S$.

Data by Gisen et al. (2015)

The data set by Nienhuis et al. (2018) did not include salt intrusion data, therefore we added a data set by Gisen et al. (2015) which does include data for the salt intrusion length. To check whether our model prediction for the salt intrusion length is reliable, the predicted salt intrusion length has to be compared to the measured salt intrusion length given by Gisen et al. (2015). Gisen et al. (2015) expanded a data base of Savenije (1993), which resulted in a data set with the measured salt intrusion length for 29 estuaries at dry moments in time (low river discharge).

Gisen et al. (2015) made use of an inflection point, which is defined as the point where the estuary changes from wave-dominated (seaward side) to tide-dominated (landward side). This means that some parameters are given at the inflection point, while we are interested in the values at the estuary mouth. The river discharge, channel depth, river width, tidal range and tidal period were directly taken from the data set, since those were not depending on this inflection point. When the distance from the estuary mouth to the inflection point is zero, it means that there is no inflection point and the width at the inflection point is equal to the mouth width. In that case, the mouth width is also directly taken from Gisen et al. (2015). However, when there is an inflection point, the mouth width is taken from Savenije (1993) when present, and otherwise it is measured using Google Earth. In the last case, the same measuring technique is used as in Nienhuis et al. (2018), where the mouth width is measured at the most downstream location where the banks still vary gradually. The slope of the estuaries was not given in the study of Gisen et al. (2015), but determined via a similar method as Nienhuis et al. (2018) by making use of Google Earth. To do so, the river was followed from the mouth at mean sea level to the point where the elevation exceeded 10 m above mean sea level. The slope was then determined by dividing the height difference of 10 m by the length of the path. For validation of the salt intrusion predictor without using the hydrodynamics and morphodynamics of the 1D numerical model, the tidal excursion length at the mouth and the convergence lengths of the width and cross-sectional area at the inflection point given by Gisen et al. (2015) were used.

So, the total data set combining the data of Nienhuis et al. (2018) and Gisen et al. (2015) consists of 101

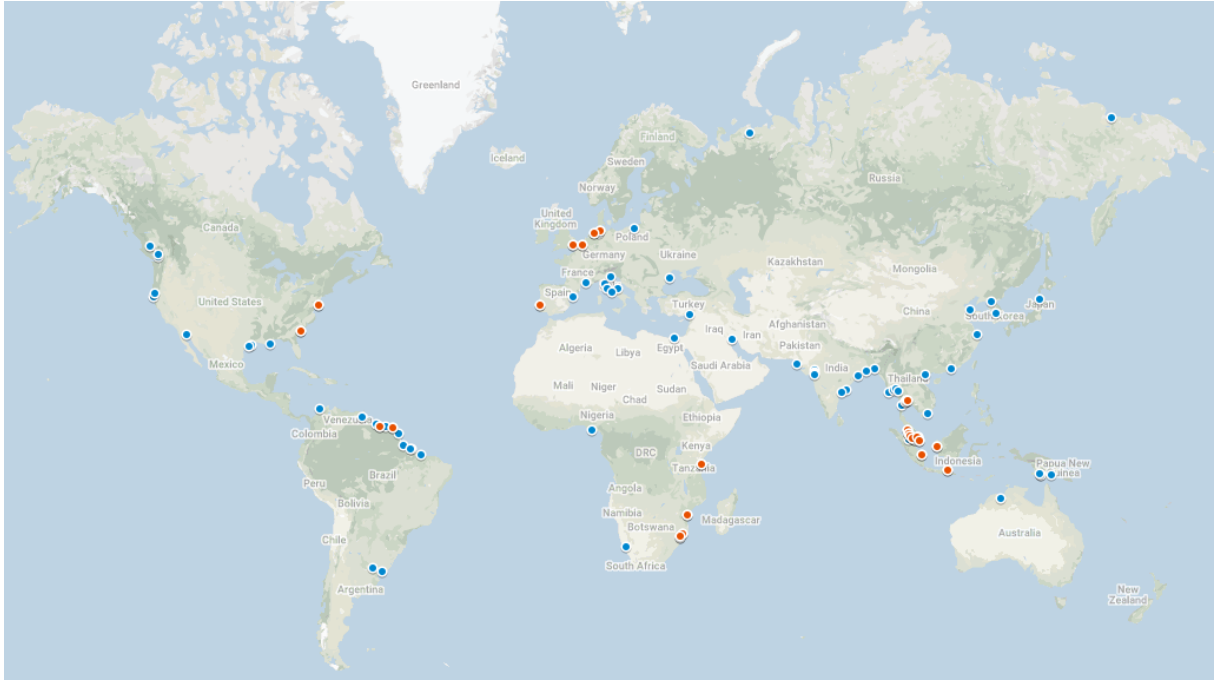


Figure 10: Estuary data set. In blue: Nienhuis et al. (2018), in red: Gisen et al. (2015).

estuaries located worldwide. A map indicating all estuaries is given in figure 10 and the data is given in table 3 in appendix B.

5 Methods

The methods consist of four different parts: 5.1) Testing the model hydrodynamics by comparing the modelled tidal prism to the tidal prism by Nienhuis et al. (2018), 5.2) Calibration of the width prediction by finding the optimal empirical calibration coefficients α and β for equation 20, 5.3) Testing the predictor for salt intrusion length by comparing it to measured salt intrusion length data of Gisen et al. (2015), and 5.4) Change the river discharge and analyze the width and salt intrusion response. A visual schedule of the model and methods is included in figure 11.

5.1 Testing the model hydrodynamics

Before using the one-dimensional tide-averaged model, the hydrodynamics of this model were tested by comparing the tidal prism to the predicted tidal prism of the very simplistic model of Nienhuis et al. (2018). The model of Nienhuis et al. (2018) assumed that the water levels in the estuary go up and down equally, neglecting tidal wave propagation. Especially for large estuaries, this is a huge simplification, which will have consequences for the calculation of the hydrodynamics, including the tidal prism. As was expected, it seemed that the 1D tide-averaged model has a better tidal prism prediction than this model by Nienhuis et al. (2018). For the complete analysis of this, see appendix C.

5.2 Calibration of width prediction

We calibrated the width prediction in the 1D tide-averaged model by comparing the modelled estuary width to the measured estuary width from Nienhuis et al. (2018). To ensure that the modelled and observed width are as close as possible to each other, the best fitting empirical coefficients (α and β) in equation 20 have to be found for the observed estuary data. The 1D tide-averaged model is run for 5 different values for α and 5 different values for β , giving 25 combinations of α and β in total. Originally, a β of 0.5 and an α of 4 were chosen in the model, since most rivers correspond to this (Janssen, 2022). Since it is expected that estuaries will require a higher β due to their tidal influence, a range of 0.55 to 0.65 was chosen for β . For α , a range of 2 to 6 was used.

The river discharge (Q_r), channel depth (h), slope (S), tidal amplitude (a_t) and tidal period (T) for the 72 estuaries of the data set of Nienhuis et al. (2018) were inserted into the 1D tide-averaged model. To see how well the width for a combination of α and β fits the observed width, the Root Mean Square Error (RMSE) was calculated. The RMSE is a widely used measure for evaluating the accuracy of models and is given by:

$$RMSE = \sqrt{\frac{\sum_{n=1}^N (\hat{y}_n - y_n)^2}{N}} \quad (24)$$

where \hat{y}_n is the predicted value, y_n is the observed value and N is the number of prediction pairs (Wang & Lu, 2018). Since absolute values will give larger errors for wider estuaries, the ratio of the modelled width against the observed width is used. This makes $\hat{y}_n = B_{mod}/B_{obs}$ and $y_n = 1$ resulting in the following RMSE formulas for the river width ratio and mouth width ratio:

$$RMSE_r = \sqrt{\frac{\sum_{n=1}^N ((B_{r,mod}/B_{r,obs})_n - 1)^2}{N}} \quad (25)$$

$$RMSE_m = \sqrt{\frac{\sum_{n=1}^N ((B_{m,mod}/B_{m,obs})_n - 1)^2}{N}} \quad (26)$$

When the modelled width is equal to the observed width, the ratio B_{mod}/B_{obs} becomes 1 and the RMSE becomes 0. So, the lower the RMSE, the better the model fits the data.

The RMSE was calculated for the river width (upstream boundary) and the mouth width (downstream boundary). Since this will result in two RMSEs, the total RMSE is calculated that combines the RMSE at the river with the RMSE at the mouth:

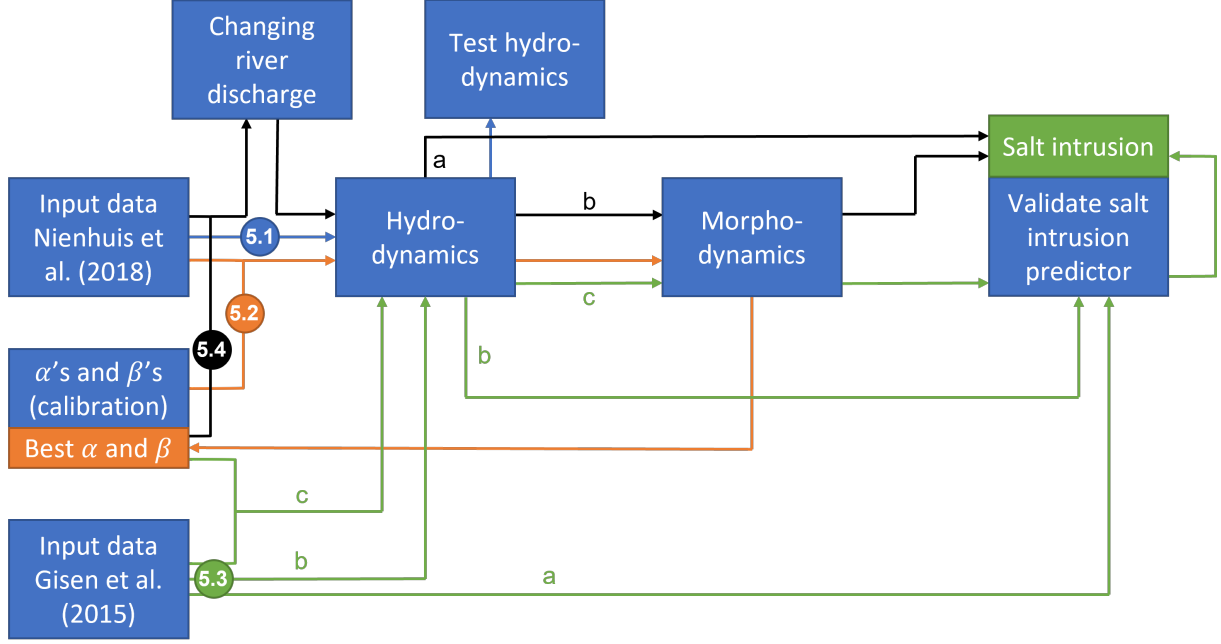


Figure 11: Schedule of model and methods. In blue (5.1): validation of the hydrodynamics; in orange (5.2): calibration of width prediction by finding the best α and β ; in green (5.3): validation of salt intrusion length predictor by a) directly inserting the input data in the salt intrusion equations, b) by using the hydrodynamics of the 1D tide-averaged model, c) by using both the hydro- and morphodynamics of the 1D tide-averaged model; in black (5.4): changing the river discharge and a) calculate the hydrodynamics and its salt intrusion response and b) calculate the hydro- and morphodynamics and its salt intrusion response.

$$RMSE_{total} = \sqrt{\frac{(RMSE_r + RMSE_m)^2}{2}} \quad (27)$$

The lowest total RMSE gives the most optimal combination of α and β .

With the previously described method the river width and mouth width are analyzed separately. To check the best predicted amount of convergence as well, the width ratio B_m/B_r is used. In that case, the predicted ratio \hat{y}_n becomes

$$\hat{y}_n = \frac{(B_m/B_r)_{mod}}{(B_m/B_r)_{obs}} \quad (28)$$

while y_n is still 1, giving the following formula for the RMSE:

$$RMSE_{B_m/B_r} = \sqrt{\frac{\sum_{n=1}^N \left(\left(\frac{(B_m/B_r)_{mod}}{(B_m/B_r)_{obs}} \right)_n - 1 \right)^2}{N}} \quad (29)$$

Again, the lower the RMSE, the better the fit.

5.3 Predictor for salt intrusion length

When the best values for the empirical coefficients α and β for the width prediction are found, it is assumed that they can be used for all estuaries and the 1D tide-averaged model can be expanded with a salt intrusion predictor. We used the salt intrusion length predictor of Savenije (1993), see section 2.2, where the salt intrusion length at high water slack L^{HWS} is calculated by:

$$L^{HWS} = L_a \ln \left(\frac{1}{\beta_m} + 1 \right) \quad (30)$$

where β_m is a positive number depending on the Van der Burgh's coefficient K and mixing coefficient α_m among others. Gisen et al. (2015) revised those predictive equations for the salt intrusion of Savenije (1993) and came up with some new improved empirical formulas. However, those new equations are more complex and require more input arguments, of which some cannot be directly taken from the 1D tide-averaged model. This leads to much more uncertainties and a worse fit for the salt intrusion length. For this analysis, see appendix D.

To see whether the method by Savenije (1993) can be applied to the 1D tide-averaged model, we tested the equations of Savenije (1993) in three ways. First of all, we just implemented the data of Gisen et al. (2015) into the equations of Savenije (1993) and compared the outcome of the calculated salt intrusion length to the measured salt intrusion length (step 5.3a in figure 11). Gisen et al. (2015) made use of an inflection point, which is the point where the estuary changes from wave-dominated to tide-dominated geometry (see appendix D). The assumption is made that the salt intrusion reaches at least till the inflection point, which means that the length from the mouth to the inflection point has to be added to equation 30.

After that, the hydrodynamics were taken from the 1D tide-averaged model, while the morphology was kept constant with a width profile similar to the width profile used by Gisen et al. (2015) (step 5.3b in figure 11). Since the width convergence length and river width were given in the study of Gisen et al. (2015) and the mouth width is also known (see table 3 in appendix B), the length of the estuary can be determined by:

$$L_e = -L_b \ln \left(\frac{B_r}{B_m} \right) \quad (31)$$

To make sure the tide dampens out before it reflects at the upstream boundary, a river part is added with the same length and a constant river width. To get the same constant estuary width profile as used by Gisen et al. (2015), the width formula yields:

$$B = B_m \exp \left(- \frac{x}{L_b} \right) \quad (32)$$

Since we want to replicate the width profile by Gisen et al. (2015), B_m is in this case the width at the inflection point and only the part upstream of the inflection point is modelled. Therefore, we still have to add the distance from the mouth to the inflection point to the salt intrusion length. By taking the hydrodynamics of the 1D tide-averaged model, the tidal excursion length at the mouth E_m will change and can be calculated by:

$$E_m = \frac{v_m T}{\pi} \quad (33)$$

with v_m is the tidal velocity amplitude at the estuary mouth (m s^{-1}), which follows from the harmonic analysis in the model (Parsa & Etemad-Shahidi, 2010).

Lastly, runs were done with an adjusting width following the empirical hydraulic geometry relation with the best fitting empirical coefficients α and β (equation 20, step 5.3c in figure 11). The intermediate step of taking the hydrodynamics of the 1D tide-averaged model, but the morphology still from Gisen et al. (2015) (step 5.3b) was made to see the direct effect of a changing morphology. Equation 32 is rewritten to calculate the width convergence length:

$$L_b = \frac{x_b}{\ln(B/B_m)} \quad (34)$$

where x_b is defined as the distance of the estuary mouth till the boundary where the width is still larger than the river width, so it is the part where $B > B_r$. The width convergence length L_b and cross-sectional area convergence length L_a are often very close or similar to each other, see figure 12. Since the bed level is constant, the depth differences in the upstream part are much smaller than the width differences and L_a will be taken the same as L_b (Dronkers, 2017).

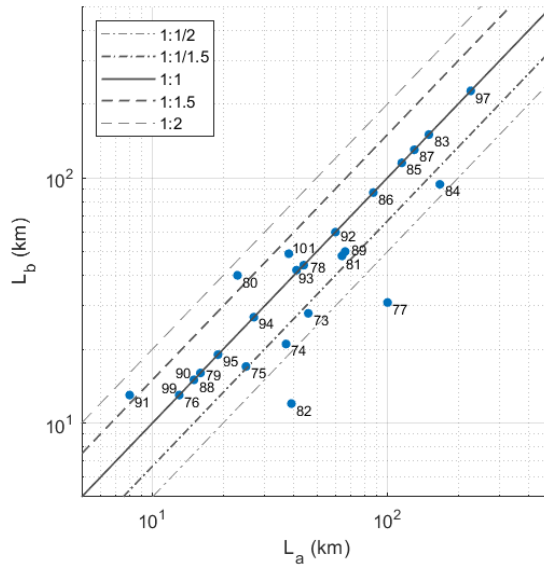


Figure 12: Convergence lengths by Gisen et al. (2015). Numbers and corresponding estuary names can be found in table 3 of appendix B.

To test the salt intrusion length predictor, the salt intrusion calculated by the model was compared to the measured salt intrusion length given in Gisen et al. (2015). If the modelled and measured salt intrusion lengths are close to each other, it is assumed that the method by Savenije (1993) is valid and can be used for other estuaries as well.

5.4 Changing the river discharge

River discharge changes can be due to seasonal fluxes, climate change or to changes upstream in the river like dam construction or more intense irrigation, see section 2.3. To simulate river discharge changes, the 1D tide-averaged model is run for river discharges of 5%, 15%, 25%, 50%, 75%, 100%, 125%, 150%, 175% and 200% of the yearly averaged river discharge. This was only done for the estuaries included in the data set by Nienhuis et al. (2018), since this data set contains yearly averaged discharge data. The data set of Gisen et al. (2015) holds very low discharge data, which makes a further decrease in river discharge not always realistic.

On the short term, it is assumed that changes in river discharge only change the hydrodynamics without changing the morphology of the estuary. For the short term simulations, the width is kept constant and is equal to the equilibrium width profile on the long term for the yearly averaged river discharge (100%). On a longer timescale, it is expected that the width profile of the estuary will change as well with a change in river discharge. Both the effects on the morphology and the salt intrusion are investigated and it is tried to find a relation between the width and river discharge on the long term and between the salt intrusion length and river discharge on both the short term and long term. To do so, we will use the normalized river discharge $Q_{r,ratio}$, which is the fraction of the yearly averaged river discharge (ranging from 0.05 to 2). The normalized width ($B_{r,ratio}$ and $B_{m,ratio}$) is the width divided by the width belonging to a yearly averaged river discharge. So, at a river discharge of 100% (yearly averaged), the normalized width ratio will be 1. The same is done for the salt intrusion length, where the normalized salt intrusion length is the new salt intrusion length divided by the original salt intrusion length at 100% river discharge. In formulas, this will read as:

$$Q_{r,ratio} = \frac{Q_r}{Q_{r,ave}} \quad (35)$$

$$B_{ratio} = \frac{B}{B_{ave}} \quad (36)$$

$$L_{ratio}^{HWS} = \frac{L^{HWS}}{L_{ave}^{HWS}} \quad (37)$$

with $_{ave}$ stands for the value belonging to the original situation of yearly averaged river discharge.

Since it is assumed the width only changes on the long term, the width response to changing river discharge only applies to the long term. Since the river width is assumed to be in equilibrium and there is no tidal influence far upstream in the river (equation 21), the equation for the river width ratio becomes:

$$\frac{B_r}{B_{r,ave}} = \frac{\alpha Q_r^\beta}{\alpha Q_{r,ave}^\beta} \quad (38)$$

which, in combination with equations 35 and 36, can be rewritten to:

$$B_{r,ratio} = Q_{r,ratio}^\beta \quad (39)$$

where $B_{r,ratio}$ and $Q_{r,ratio}$ are dimensionless, since these are ratios. In contrary to the river width, the mouth width depends on both the river discharge and the tidal discharge (equation 20). Therefore, the equation for the normalized mouth width will be:

$$B_{m,ratio} = \left(\frac{Q_r + Q_t}{Q_{r,ave} + Q_{t,ave}} \right)^\beta \quad (40)$$

Since we are interested in the effect of the river discharge on the mouth width, this formula is rewritten to:

$$B_{m,ratio} = Q_{r,ratio}^{\beta_B} \quad (41)$$

where β_B is a non-dimensional coefficient which defines the slope in the $Q_{r,ratio}$ - $B_{m,ratio}$ loglog-plot. This β_B will be found by fitting a first-order polyfit line through the modelled mouth width ratio.

Lastly, we will try to find a relation for each estuary between the salt intrusion length and the river discharge of the same form:

$$L_{ratio}^{HWS} = Q_{r,ratio}^{-\beta_L} \quad (42)$$

where β_L is a non-dimensional coefficient which defines the slope in the $Q_{r,ratio}$ - L_{ratio}^{HWS} loglog-plot. This is done for the short term, when there is no morphology change, and for the long term, when there is a hydro- and morphodynamic change. After that, the salt intrusion response to changing river discharge and changing morphology is analyzed for a river-dominated delta (the Mississippi), a mixed estuary (the Amazon) and a tide-dominated estuary (the Thames) (see figure 2).

6 Results

The results of the model runs are displayed and shortly discussed in this section. First of all, the results of the width calibration will be shown and the combination of α and β showing the best fit will be given. Secondly, the results for the predictor for the salt intrusion length compared to the measured salt intrusion length by Gisen et al. (2015) will be displayed. Then, the morphological response of estuaries to changing river discharge will be discussed. Lastly, the effects of changing river discharge on salt intrusion will be discussed on both the short term and long term and for three kind of systems ranging from river-dominated to tide-dominated.

6.1 Calibration of width prediction

When combining the Root Mean Square Error (RMSE) of the river width ratio $B_{r,mod}/B_{r,obs}$ and the mouth width ratio $B_{m,mod}/B_{m,obs}$ for different combinations of α and β in the total RMSE ($RMSE_{total}$) of equation 27, the color-plot in figure 13 is the result. When β becomes larger, α becomes smaller for a good fit and vice versa. From this plot, it follows that the best fit occurs for $\alpha = 6$ and $\beta = 0.575$ with a RMSE of 0.466. Since the RMSE of a ratio is calculated, the value does not have a unit. A RMSE of 0.466 means that there is on average a difference of 46.6% between the modelled and observed width. The combinations $\alpha = 5$ and $\beta = 0.6$ and $\alpha = 4$ and $\beta = 0.625$ have RMSE values of 0.470 and 0.483 respectively, meaning that these combinations of α and β are almost as good.

We also looked at the RMSE of the river width ratio ($RMSE_r$, equation 25) and mouth width ratio ($RMSE_m$, equation 26) separately, these results are given in figures 28 and 29 in appendix E. For the mouth width, the best fitting β is larger than for the river width, which makes sense since the mouth width needs to be wider. For the mouth width, the best combination of α and β is $\alpha = 5$ and $\beta = 0.6$ with $RMSE_m = 0.498$, while for the river width the best combination is $\alpha = 6$ and $\beta = 0.55$ with $RMSE_r = 0.392$. The values of the RMSEs indicate that the uncertainties in the mouth width prediction are higher than in the river width prediction.

When the RMSE of the width ratio B_m/B_r is taken, the same combination of $\alpha = 6$ and $\beta = 0.575$ as for the total RMSE seems to be best, see figure 14. Here, the value for the $RMSE_{B_m/B_r}$ is 0.456, meaning that there is on average a 45.6% difference between the modelled width ratio and observed width ratio, meaning that the convergence is on average under- or overestimated by 45.6%.

The $RMSE_{total}$ that was calculated for the width prediction model of Nienhuis et al. (2018) was 0.505, which means that our width prediction is slightly closer to the observed width. The combination $\alpha = 6$ and $\beta = 0.575$ will be used further in this study.

The modelled and observed river width, mouth width and width ratio for the best combination of $\alpha = 6$

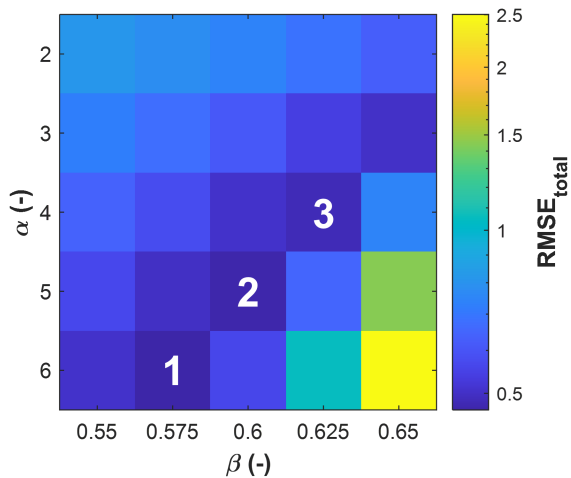


Figure 13: Total RMSE for river width and mouth width combined, 1 to 3 indicates the top 3 lowest RMSE for the combinations of α and β .

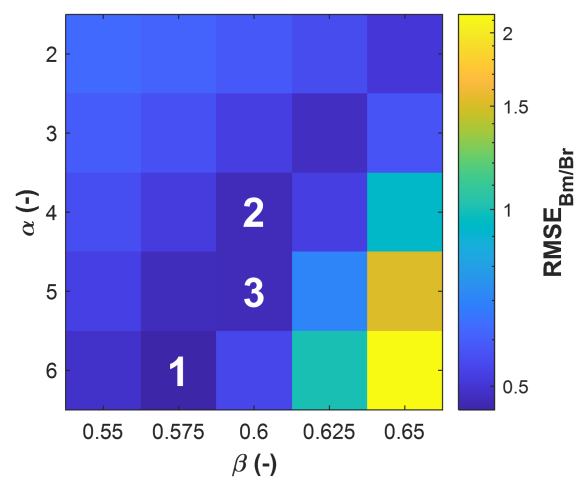


Figure 14: RMSE for width ratio B_m/B_r , 1 to 3 indicates the top 3 lowest RMSE for the best combinations of α and β .

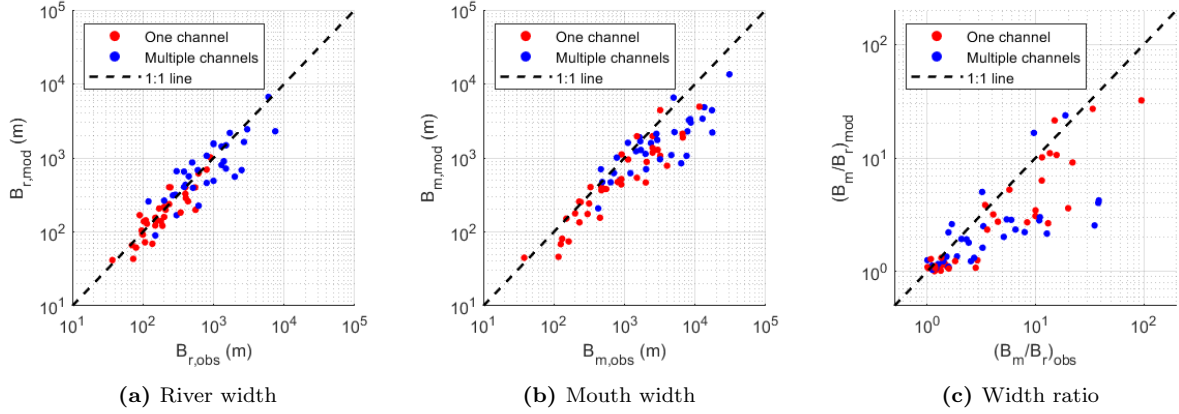


Figure 15: Best fits for the river width, mouth width and width ratio ($\alpha = 6$ and $\beta = 0.575$).

and $\beta = 0.575$ are plotted in figures 15a, 15b and 15c. As can be seen, the scatter cloud for the river width (figure 15a) is around the perfect agreement line. Although differences between the observed and modelled width might be up to a factor 5 more or less, there is no structural over- or underestimation in the river width meaning that there is no bias. However, for the mouth width in figure 15b, the modelled width is often smaller than the observed width, meaning that there is a bias in the mouth width prediction. This can also explain the underestimation in the modelled width ratio B_m/B_r in figure 15c. This indicates that the modelled convergence is less than the observed convergence. We will still use this width prediction with $\alpha = 6$ and $\beta = 0.575$, however, this underestimation has to be kept in mind.

6.2 Testing the predictor for salt intrusion length

When the data of Gisen et al. (2015) is inserted directly in the salt intrusion predictor method of Savenije (1993), the calculated L_{HWS} for every estuary falls within a factor 2 range from the measured L_{HWS} , as can be seen in figure 16a. The RMSE for the ratio $L_{calc}^{HWS}/L_{obs}^{HWS}$ is 0.289. A maximum error of a factor 2 in combination with the low RMSE means that the method of Savenije (1993) works very well when the data of Gisen et al. (2015) is inserted.

When the hydrodynamics are taken from the 1D tide-averaged model, but the width profile is kept similar to the width profile used by Gisen et al. (2015), figure 16b is the result. Most estuaries fall within the factor 2 range and the RMSE of the ratio between the modelled and observed salt intrusion length becomes 0.274, meaning that the method of Savenije (1993) still works very well when the hydrodynamics are taken from the 1D tide-averaged model. In comparison to figure 16a, the modelled salt intrusion length has become smaller for most estuaries. To include the hydrodynamics, only the tidal excursion length E has changed (figure 30 in appendix E). The modelled tidal excursion length in the 1D tide-averaged model is smaller compared to the data of Gisen et al. (2015) (except for the Chao Phya) due to a lower modelled tidal velocity amplitude at the mouth than expected. A decrease in tidal excursion length indicates that water particles travel less far and the sea water will intrude less far, causing the salt intrusion length to become smaller.

When both the hydro- and morphodynamics are taken from the 1D tide-averaged model, figure 16c is the result. The scatter cloud around the perfect agreement line becomes wider and the RMSE of the $L_{mod}^{HWS}/L_{obs}^{HWS}$ ratio increases to 0.756, meaning that the prediction is less reliable. However, differences are still within a factor 3 range and for many estuaries even within the factor 2 range, and no bias is found. Therefore, this fit is considered to be good and the method of Savenije (1993) will be applied in the 1D tide-averaged model to calculate the salt intrusion length.

For three estuaries the 1D tide-averaged model was not able to simulate the hydro- and morphodynamics: the Incomati, Eems and Rompin. The data set of Gisen et al. (2015) contains data with very low river discharges (dry moments) in combination with wide width profiles of the average situation. When we look at the Eems estuary, the river discharge in the data set of Gisen et al. (2015) is only $10 \text{ m}^3 \text{ s}^{-1}$, while the yearly averaged discharge is $110 \text{ m}^3 \text{ s}^{-1}$ (van Leussen, 1999). The estuary mouth width is still over 30 km. This means that the discharge will be too low for the width and the water level in the 1D tide-averaged model will drop below the bed level, which will result in an error of the model. However,

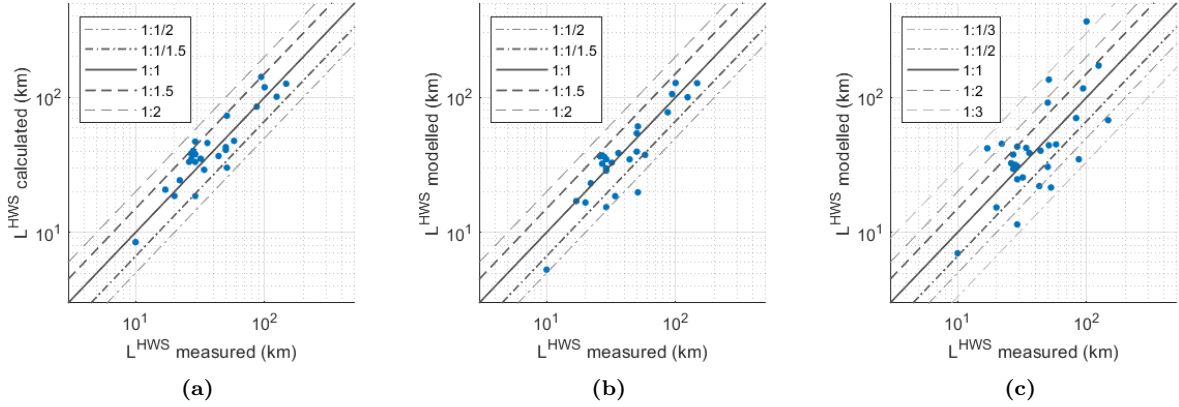


Figure 16: Calculated or modelled salt intrusion length against measured salt intrusion length. (a) Data from Gisen et al. (2015) directly in method of Savenije (1993), (b) Hydrodynamics from 1D tide-averaged model, morphology from Gisen et al. (2015), (c) Hydro- and morphodynamics from 1D tide-averaged model.

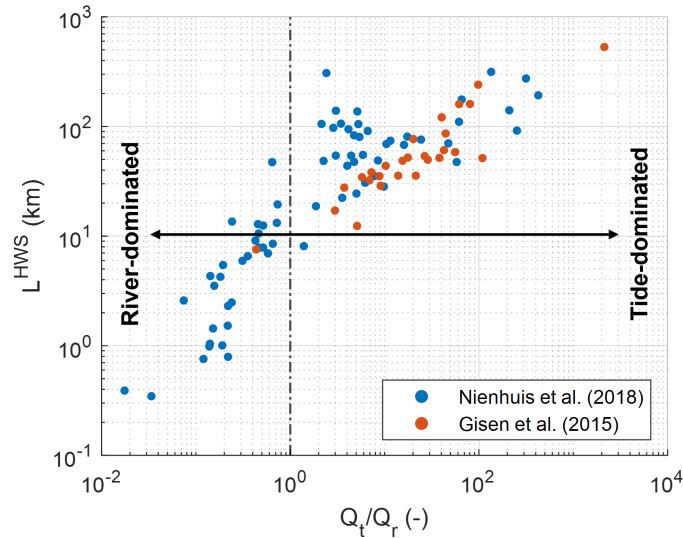


Figure 17: The salt intrusion length for the systems in the data sets of Nienhuis et al. (2018) and Gisen et al. (2015) against the tide dominance ratio.

the data set by Nienhuis et al. (2018) contains yearly averaged river discharge data, so this problem will probably not occur within this data set. Furthermore, when we take the width from the empirical width prediction, the model will adapt the width to the low river discharge, which will probably solve the errors.

6.3 Salt intrusion length prediction

Since the salt intrusion length method by Savenije (1993) showed a good prediction of the salt intrusion length in the 1D tide-averaged model for the estuaries in the data set of Gisen et al. (2015), the salt intrusion length was also calculated for all systems in the data set of Nienhuis et al. (2018). The salt intrusion length for the original situation with a yearly averaged river discharge against the tide dominance ratio of all systems is plotted in figure 17. The tide-dominance ratio $I = Q_t/Q_r$ and salt intrusion length for the yearly averaged river discharge are also given in table 4 in appendix F. With an increase in tide-dominance ratio, the salt intrusion length becomes longer. Following figure 17, typical values for the salt intrusion length of tide-dominated systems are in the order of 10^2 or 10^3 km, while the salt intrusion length for river-dominated systems is in the order of 1 to 10 km. This means that due to the large river-influence of river-dominated systems, the transport of salt water into the estuary system by the tide is limited.

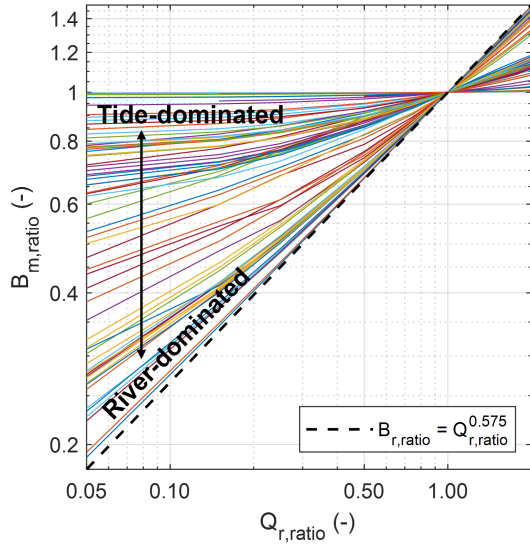


Figure 18: Morphological response of the mouth width to changing river discharge, the river width response is given by the dotted line. When the slope of the line is close to 0.575, the estuary is river-dominated (delta), while a slope close to 0 means that the estuary is tide-dominated.

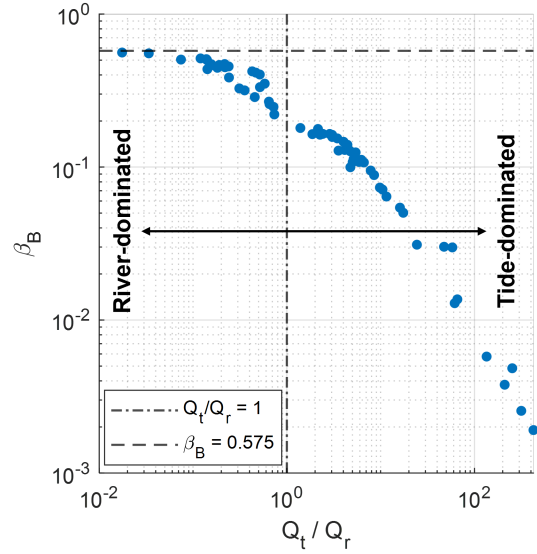


Figure 19: The power in the relation between $Q_{r,ratio}$ and $B_{m,ratio}$, the slope of the lines in figure 18. The closer β_B is to 0.575, the more river-dominated the estuary is.

6.4 Width response to changing river discharge

On a short time scale, we assumed that there would be no morphological adjustment. Therefore, in this section, we will discuss the morphological response to changing river discharge on a long term. Since we used an equilibrium river width as boundary condition (see equation 21), the normalized river width $B_{r,ratio}$ depends on the normalized river discharge $Q_{r,ratio}$ via the same equation for every estuary, see the dotted line in figure 18. Note that it is a log-log plot, meaning that the slope is the exponential power in the equation. Following the model calibration (section 6.1), $\beta = 0.575$ gives

$$B_{r,ratio} = Q_{r,ratio}^{0.575} \quad (43)$$

For example, when the river discharge decreases to 50% of the original yearly averaged discharge, the river width will decrease by 33% on the long term. Of course, the absolute change in river width differs for every estuary.

Unlike the change in relative river width, the change in relative mouth width is different per estuary, see all the colored lines in figure 18. This means that also the power β_B in equation 41 changes, see figure 19. For some systems the mouth width ratio becomes very close to the line $B_{m,ratio} = Q_{r,ratio}^{0.575}$, meaning that the river width and mouth width will change with almost the same rate. Those systems are river-dominated and the river discharge has a large influence on both the river width and mouth width. There is no line for the mouth width ratio that is exactly equal to the line of the river width ratio with a slope of 0.575, since there will always be a (very small) tidal influence affecting the mouth width. When the estuary is very tide-dominated, even a large change in river discharge does not significantly affect the morphology of the estuary, since the tidal discharge is large enough to keep the mouth width wide. In this case, β_B becomes very small. For mixed estuary systems, both river and tides are important and β_B falls in between river- and tide-dominated systems.

So, a change in river discharge that holds for a few weeks will not significantly affect the morphology. When the river discharge changes for years or decades, the width will start to change. The river width will decrease via the formula $B_r = B_{r,ave} Q_{r,ratio}^{0.575}$, while the mouth width changes with a different rate for every estuary depending on the power β_B , which is given for every estuary in table 4 in appendix F.

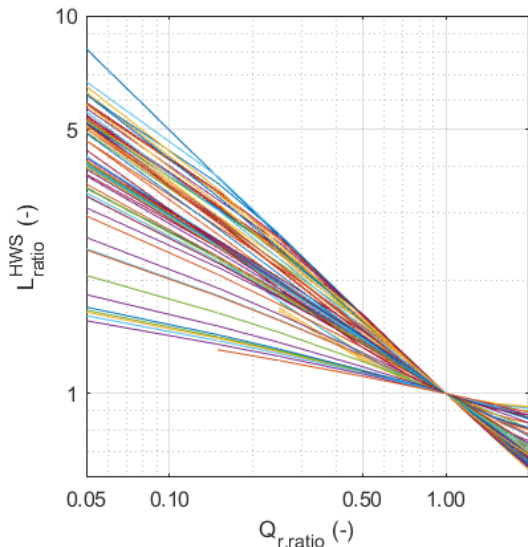


Figure 20: Salt intrusion change in response to changing river discharge on the short term (no morphodynamic change). Every line represents an estuary.

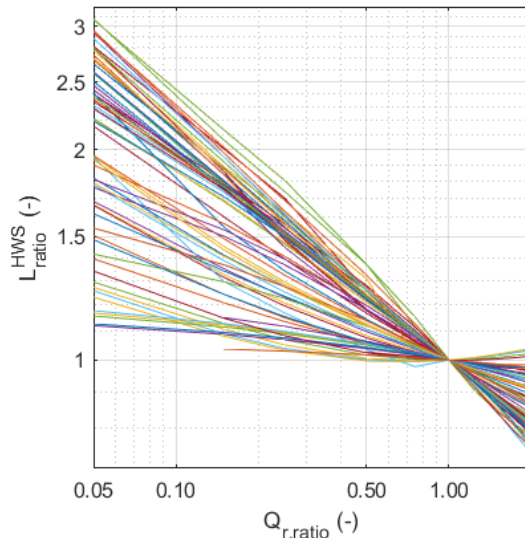


Figure 21: Salt intrusion change in response to changing river discharge on the long term (hydro- and morphodynamic change). Every line represents an estuary.

6.5 Effect of changing river discharge on salt intrusion

The underlying hypothesis of this thesis is that a change in river discharge and the possible morphological response to that on the long term will affect the salt intrusion. In this section, we will look at the salt intrusion response on the short term and on the long term and compare them. On the short term, in response to changing river discharge, the hydrodynamics like the tidal discharge, tidal velocity amplitude and tidal excursion length will change. Figure 20 gives the change in salt intrusion length compared to the river discharge ratio on the short term. As can be seen, the salt intrusion length increases for a decrease in river discharge and vice versa. With a lower river discharge, the friction between the river and the tide will decrease, meaning that the tide can penetrate further into the estuary which increases the tidal prism. Furthermore, the fresh water supply into the estuary decreases, causing more salinization of the system. There are differences between estuaries, where some estuaries have a very large relative increase in salt intrusion length (up to a factor 8 for 5% river discharge), while others have a small relative increase in salt intrusion length (not even up to a factor 2 for 5% river discharge). The slope defines the power β_L in equation 42 and is different per estuary and different on the short term and long term, the results are given in table 4 in appendix F.

At a longer time scale, when the estuary can narrow or widen, the salt intrusion length still depends on the river discharge, but less directly, see figure 21. For most estuaries, the salt intrusion length is still decreasing for a larger river discharge due to the counteracting effect of the river discharge. However, for some estuaries the salt intrusion length increases again when the river discharge becomes larger than the yearly averaged discharge. This can be explained by the width and depth of the estuary. Although the bed level is fixed, the water level can still fluctuate. When the river discharge is larger, there is more water coming through the estuary and the width and depth will increase. When the width and depth increase, there is less friction between the tide and the bed and the tide can propagate further. When this effect is larger than the counteracting effect of the river discharge, it means that salt water is brought further into the estuary and the salt intrusion length will increase. For some estuaries, both on the short term and long term, a very low river discharge of 5 to 25% of the yearly averaged discharge resulted in drying up of the estuary making it impossible to calculate the salt intrusion length.

River-dominated system

For the yearly averaged river discharge, the Mississippi has a tide-dominance ratio (Q_t/Q_r) of 0.07, meaning that the Mississippi is river-dominated. The width convergence is very small for river-dominated systems, as can be seen in figure 22a, where the width profile is almost straight. The salt intrusion length

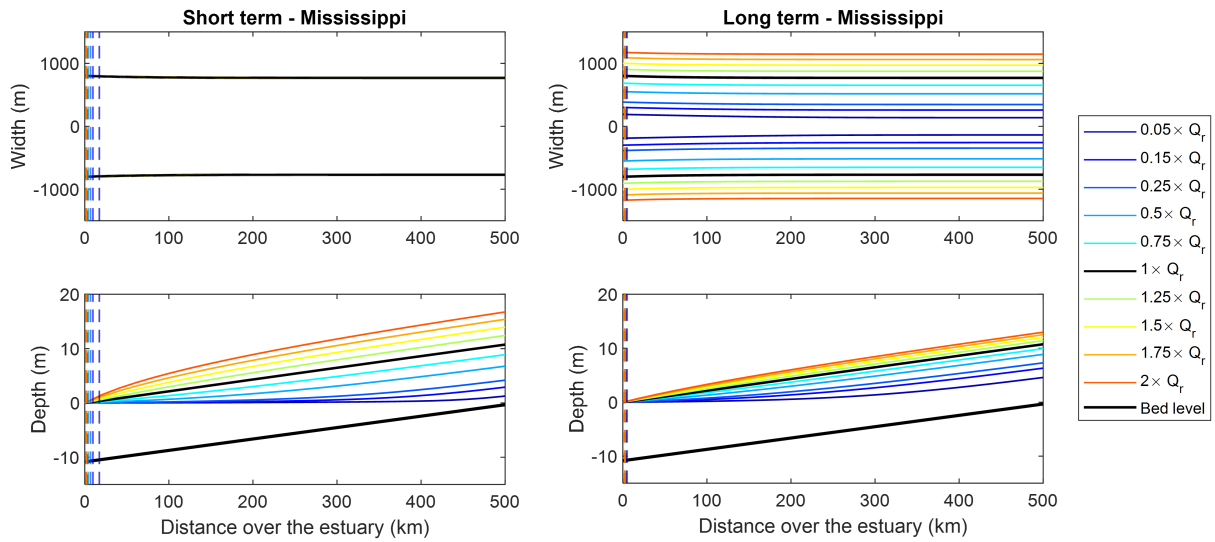
is very small due to the river-dominance, but is slightly larger on the short term than on the long term. Figure 23a displays the salt intrusion development for different river discharges in the Mississippi. On the short term, the change in river discharge will have a large effect on the salt intrusion length, indicated by the highly negative power (large β_L). When the river discharge goes down, the friction between river and tide goes down and the tide can intrude further increasing the salt intrusion length. For a hypothetical case where the river discharge decreases to 15%, the salt intrusion length becomes almost 3.5 times larger on the short term. However, if the lowering of the river discharge persists, the river width and mouth width will narrow to almost the same rate (see section 6.4). The extreme narrowing of the mouth width causes that the tide can enter the estuary less easily and more friction with the bed occurs, meaning that the salt intrusion length will drop. In the case of a river discharge decrease to 15%, the salt intrusion length will go from 3.5 times the original length on the short term to 1.5 times the original length on the long term. Generally, for river-dominated systems, the exponent β_L will be relatively large on the short term (about 0.3 – 0.7) and relatively small on the long term (about 0.05 – 0.3), see figure 24.

Mixed system

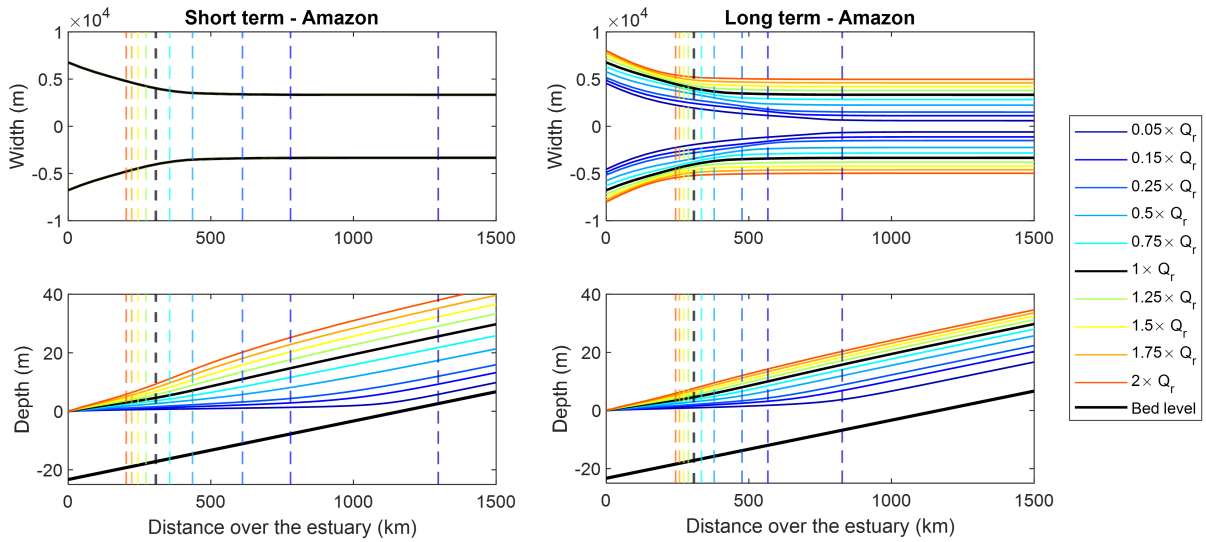
With a tide-dominance ratio of 2.4, the Amazon can be considered as a mixed system with a very small tendency towards tide-dominance. This system shows much more convergence than the river-dominated Mississippi (figure 22b). If the river discharge decreases, the estuary becomes narrower and more funnel-shaped. On the short term, β_L is smaller for the Amazon (0.50) compared to the Mississippi (0.65). This is caused by the larger river-dependence of the Mississippi, causing that a change in river discharge will have larger effects on the hydrodynamics. On the long term, exactly the opposite is observed, since β_L is larger for the Amazon (0.33) than for the Mississippi (0.18). This is caused by the differences in width of the estuary mouth. The Mississippi mouth narrowed so much that the tide can barely enter the estuary. The Amazon mouth narrows, but is still wide due to the convergence. This makes it easier for the tide to propagate into the estuary and the salt intrusion length will stay larger on the long term. So, following figure 24, the mixed systems have a relatively large β_L on the short term (0.4 – 0.6) and on the long term (0.25 – 0.4).

Tide-dominated system

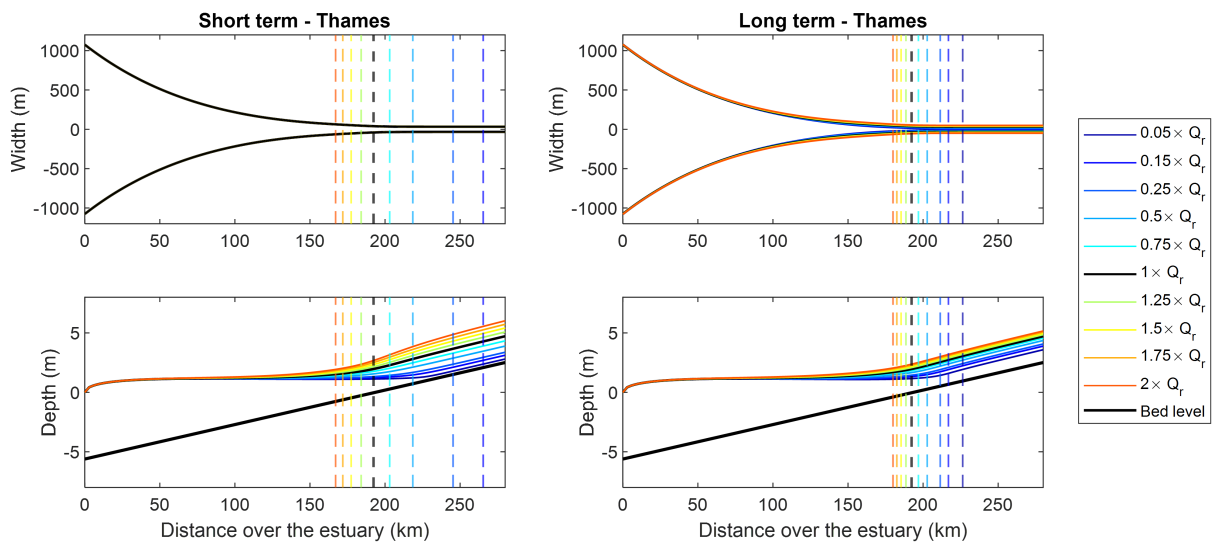
The Thames is a tide-dominated system with a tide-dominance ratio of 425. The tide-dominance causes that the estuary has a large convergence and is funnel-shaped (figure 22c). Due to the small river influence, the estuary will not narrow or widen a lot for a change in river discharge. The salt intrusion length is relatively large for the estuary size. Following figure 23c, β_L for the short term and the long term is very small due to the small river influence causing that a change in river discharge will not have large effects. The difference between β_L for the short and long term is also small, caused by the very small morphology change. Typical values of β_L for tide-dominated estuaries are 0.15 – 0.25 on the short term and 0.02 – 0.1 on the long term (figure 24).



(a) River-dominated system.



(b) Mixed system.



(c) Tide-dominated system.

Figure 22: Morphological response and salt intrusion on the short term and long term for a river-dominated, mixed and tide-dominated system. The dotted lines indicate the maximum salt intrusion length.

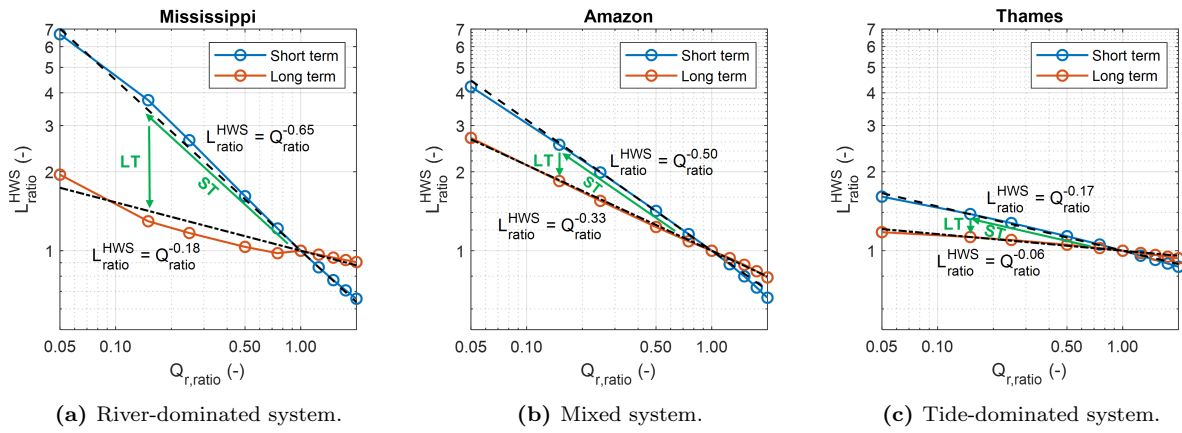


Figure 23: Relative salt intrusion length as function of river discharge ratio at the short term and long term.

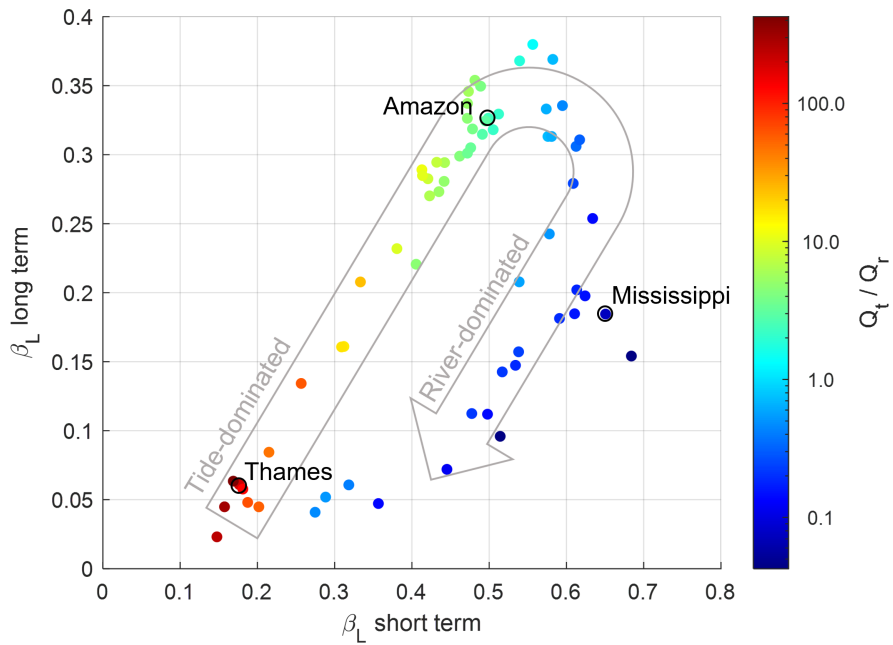


Figure 24: Exponent β_L of the river discharge as power function for the salt intrusion length for the short and long term compared to river- and tide-dominance.

7 Discussion

7.1 Estuarine hydrodynamics and morphology

We assumed changing hydrodynamics and a constant morphology on the short term, while the morphology was assumed to change as well on the long term. This raises the question: what timescales belong to the so called "short term" and "long term"? For changes in morphology, Zhou et al. (2017) stated that the interesting timescale is decades to millennia, which they also called the geomorphological timescale. In the Ord river, due to river damming upstream, large river floods were suppressed and the estuary started silting up (Wolanski et al., 2001). The East Arm of the Ord river now appears to be geomorphologically unstable due to the human activities. Numerical studies suggest that it may take at least 100 years for the East Arm of the Ord river to reach a new equilibrium (Wolanski et al., 2001). Jeuken et al. (2003) determined the morphological timescale of the Humber to be in the order of 35 years, while the morphological timescale for the Westerschelde was determined to be in the order of 100 years. This indeed suggests that the timescale to reach a new morphologic equilibrium will be at least decades to centuries. Furthermore, Jeuken et al. (2003) stated that in the Humber and Westerschelde estuaries, the start of the morphological response lags about 3 to 5 years behind the hydrodynamic forcing. This means that the hydrodynamics will change within those 3 to 5 years, but the morphology will not significantly change. Zhou et al. (2017) also found a time lag between the hydrodynamics and morphology change. This suggests that the river discharge changes due to the seasons will affect the hydrodynamics, but not the morphology. So, the short timescales have a maximum of some years, while the long timescales are typically decades to millennia (Wolanski et al., 2001; Jeuken et al., 2003; Zhou et al., 2017). Of course, the time it takes to start the morphological change and to reach a new morphological equilibrium depends on many factors such as the amount of river discharge change, the size of the estuary, the estuary dynamics and boundary conditions, which makes that the exact timescales differ per estuary.

The 1D tide-averaged numerical estuary model that was used in this research, was originally made and adapted to simulate the hydro- and morphodynamics of one channel systems without bifurcations (Iwantoro et al., 2021; Janssen, 2022). During this thesis, it was demonstrated that the model has a wider applicability. The tidal prism and width prediction were slightly better than the predictions by the very simplistic model of Nienhuis et al. (2018). For multiple channel systems that were simulated as one channel systems, the predictions were slightly worse than for one channel systems but still good. The tidal prism prediction for multiple channel systems deviates more from the perfect agreement line than the tidal prism for one channel systems, see figure 26 in appendix C. This is caused by the fact that multiple channel systems are often larger than one channel systems allowing the tide to propagate further through the channel which has a larger lowering effect on the tidal prism compared to the tidal prism by Nienhuis et al. (2018) (figure 27 in appendix C). For the width prediction, the prediction for multiple channel systems is also slightly worse than for one channel systems. The RMSE difference for the river width between one and multiple channel systems is 0.19 ($RMSE_{r,one} = 0.33$, $RMSE_{r,mult} = 0.52$), while the difference is 0.08 for the mouth width ($RMSE_{m,one} = 0.46$, $RMSE_{m,mult} = 0.54$). However, these differences are quite small, which leads to the assumption that the tide-averaged model works fine for multiple channel systems as well.

One limitation of the 1D tide-averaged model that was already found during the testing of the hydrodynamics, includes that the model does not work for very short and steep estuaries. For the data set of Nienhuis et al. (2018), it means that the 1D tide-averaged model gives an error for the Homathko, Var, Waipaoa and Klinaklini rivers. For example, the Homathko (Canada) has a length of 1.5 km and a slope of 2.1×10^{-3} . The Var has an even smaller length of 480 m and is almost straight-canalized since it ends in the city of Nice, France (Nienhuis et al., 2018). All four rivers have a relative short way from their source in the mountains to their mouth in the sea causing their steep slopes. The model does not work for those estuaries since the water depths become very shallow and the flow velocities very large. This results in a high Froude number ($Fr = \bar{u}/\sqrt{gh}$), which means that the flow goes towards supercritical flow (Retsinis & Papanicolaou, 2020). The model is not able to handle this, since the water level will drop below the bed level. For the Waipaoa and Klinaklini, it seemed that the error disappears for certain combinations of α and β when the width is adjustable. The best fitted combination of $\alpha = 6$ and $\beta = 0.575$ includes the Klinaklini river, but still excludes the Waipaoa. When the river discharge is decreased, the errors occur again for the Klinaklini. Therefore, we decided to leave those four estuaries out of the results.

The root mean square error (RMSE) calculated during the width calibration does not account for biases in the model. The RMSE calculates the error based on the deviation of the predicted values to the

observed values regardless of the deviation being in the positive or negative direction, which makes the method sensitive to biases (Wang & Lu, 2018). Indeed, a bias was found between the observed and modelled mouth width, often underestimating the modelled mouth width resulting in an underestimation of the convergence as well (figures 15b and 15c). During the calibration, it seemed that $\beta = 0.575$ and $\alpha = 6$ gave the best fit for equation 20. However, many researchers found a higher β for equation 20 of around 0.7 for tide-influenced estuary systems (Langbein, 1963; Myrick & Leopold, 1963; Rinaldo et al., 1999; Leuven et al., 2018; Janssen, 2022). Sassi et al. (2012) found a β of 0.77 in combination with an α of 2.32 for the Mahakam estuary, which is a tidally influenced river delta or a mixed system (see figure 2). For the width of rivers where there is no tidal influence, a power function of the discharge (equation 21) with an exponent β around 0.5 was often found (Lacey, 1930; Leopold & Maddock, 1953; Savenije, 1993; Cao & Knight, 1996).

Differences in convergence between river-dominated systems and tide-dominated systems are large, which indicates that it might be useful to distinguish between those systems when calibrating the width of the hydraulic geometry relation (equation 20). For a tidally influenced estuary, the convergence becomes much larger than for rivers. More width convergence can be created in the 1D tide-averaged model by increasing β (Janssen, 2022). At the same time, the formula changes from equation 21 for the river to equation 20 for the tide-influenced mouth, meaning that the tidal discharge amplitude is included, which also explains part of the convergence in the model. The data set by Nienhuis et al. (2018) contains a wide range of very convergent estuaries with (B_m/B_r) -ratios up to 100, but also system with little to no convergence, see the points that have a $(B_m/B_r)_{obs}$ close to 1 in figure 15c. The systems with very little convergence will make β lower, while the very convergent systems require a larger β . Since we wanted to develop a globally applicable model without making distinctions between estuaries beforehand, we used one value for β accepting the underestimation of the mouth width and convergence. A value for β of 0.575 might be lower than expected for tide-influenced estuaries. However, river-dominated systems are also included and β is in between 0.5 for rivers and 0.7 for tide-influenced estuaries, which makes $\beta = 0.575$ reasonable. When the interest is in a certain type of system, it might be better to distinguish between highly convergent tide-dominated systems and less convergent river-dominated systems to find the best β .

When the river discharge changes for a single estuary, the hydrodynamics (short term and long term) and morphology (long term) will change. The river width only depends on the river discharge, since we assume that there is no tidal influence far upstream in the river. Therefore, the river width ratio relates to the same power law of the river discharge ratio for every estuary (equation 43). Since the formula for the mouth width includes the tidal discharge amplitude (equation 20), the value for β_B in equation 41 changes per estuary according to the relative importance of the river and tidal discharge. If the estuary is very river-dominated, the tidal discharge is small and the formula is almost equal to the formula for the river width. Then, the width of the whole estuary is very sensitive to river discharge changes. When the tidal discharge is much larger than the river discharge, a change in river discharge barely changes the mouth width. In that case, the river width changes a lot for a different river discharge, while the mouth width will change to a much smaller extent.

One option to increase the predicted mouth width and convergence in the 1D tide-averaged model might be to let the bed level adapt. During this whole research, the bed level was kept constant over time following a linear formula (equation 23). Letting the bed level adapt can be implemented in the 1D tide-averaged model by making use of sedimentation and erosion rates or by simply using a constant width-to-depth ratio where the depth depends on the width. Janssen (2022) made use of the Exner equation for sediment conservation to change the bed level. A morphological acceleration factor was used to limit the computation time. However, this acceleration factor affects the stability of the model. Still, Janssen (2022) showed that equilibrium bed profiles were reached, which were all concave down with an increasing depth towards the mouth. This corresponds to a constant width-to-depth ratio, where the depth will exponentially increase towards the mouth since the width increases due to convergence (Janssen, 2022). The deepening and widening towards the mouth causes that the tide has less friction with the bed. Consequently, the tidal velocities can become larger, which might cause more erosion and an even larger width and depth. This can result in a positive feedback loop, meaning that the width and depth continuously increase whereby no equilibrium is reached leading to instabilities in the model. During our research, we also shortly tried a constant width-to-depth ratio. However, this indeed led to instabilities in the model, whereby the time-dependent water level dropped below the bed level for some estuaries. For the estuaries where it did work, the width prediction of the 1D tide-averaged model did not show a real improvement compared to the width prediction for a linear bed level profile. Therefore,

we decided to keep the bed profile linear. However, since Janssen (2022) found that the bed and width profiles will develop towards an equilibrium when sediment conservation laws are used, this might be interesting to implement in our model as well, see section 7.3.

During this thesis, we assumed that estuaries can narrow or widen in a free way. However, nowadays many estuaries have fixed banks by embankments. In combination with a much longer time scale for width changes than for hydrodynamic changes, this causes that many previous researchers prescribed a fixed converging width profile that does not change over time (Lanzoni & Seminara, 2002; Todeschini et al., 2008; Canestrelli et al., 2014; Bolla Pittaluga et al., 2015). However, not all estuaries have fixed banks and it is important to know how estuaries will develop on the long term. For example, the Mekong estuary has experienced bank erosion, while the Yangtze estuary experienced an overall deposition trend (Zhao et al., 2018; Hackney et al., 2020). For some estuaries, which indeed have fixed banks by human activities, it might still be important to know whether an estuary has the tendency to widen or narrow. When the estuary has the tendency to widen, this might cause erosion of the banks leading to bank instability (Leuven et al., 2021).

7.2 Salt intrusion length and change in river flow

The empirical method of Savenije (1993) that is used in this research can be applied globally and was already extensively calibrated. One of the requirements for using this method is that the estuary is alluvial and the longitudinal variation of the cross-sectional area can be described by an exponential function (Savenije, 1993). Most estuaries of the data set of Gisen et al. (2015) fulfill those requirements, except for the Delaware, Westerschelde and Tejo, which are said to be non-alluvial. Although the mouth width and convergence are often underestimated, the modelled salt intrusion length does not show a clear bias (figure 16c). If the mouth width and convergence in the model are underestimated, the width convergence length L_b is overestimated, since the distance from the mouth to the point where the width is reduced by a factor e is longer (Leuven et al., 2021). Consequently, the cross-sectional area convergence length L_a will also be overestimated, since we assumed $L_a = L_b$. With an underestimation of the mouth width, the cross-sectional area at the mouth A_m will be underestimated as well, since the depth at the mouth is constant. The combination of a too low cross-sectional area and too large cross-sectional area convergence length in equation 16 causes a lower mixing coefficient α_m . The combination of a too low mouth width and too large width convergence length results in an underestimation of the Van der Burgh's coefficient K (equation 15). Due to the underestimation of K , overestimation of L_a , underestimation of α_m and underestimation of A_m in equation 9, the coefficient β_m will become too large. So, both L_a and β_m are overestimated in equation 8. The counteraction between the fact that $1/\beta_m$ is underestimated and L_a is overestimated apparently causes that the salt intrusion length is not structurally too high or too low.

The data set by Nienhuis et al. (2018) also contains data for river-dominated deltas, which have barely converging widths. The tide dominance ratio for those river-dominated deltas ranges from 0.02 to 1, while the data set by Gisen et al. (2015) where the method was tested on only contained one system with a tide-dominance ratio below 1: the Sinnamary with $I = 0.44$ (see figure 17 and table 4 in appendix F). We should be careful when using the predictive salt intrusion length method of Savenije (1993) for river-dominated deltas, since it is not developed for those systems. Following section 6.5 and figure 24, river-dominated systems have a relatively large exponent β_L on the short term and relatively small exponent on the long term. On the short term, the opposite flow direction of the river discharge which counters the incoming tidal discharge mainly determines the salt intrusion length. On the long term, this effect is still important, but the effect of narrowing or widening is added, which determines how easily the tide can enter the estuary mouth. For river-dominated systems, the estuary narrows or widens a lot for a change in river discharge, causing that the exponents on the short term and long term show a large difference. For the systems with a large river influence, β_L has a large range, approximately 0.3 – 0.7 on the short term and 0.05 – 0.3 on the long term. This range is much wider than the range for tide-dominated systems meaning that the tide-dominated systems behave more similar to a changing river discharge than the river-dominated systems. For every tide-dominated system, a change in river discharge has little influence, which causes that the exponent is low for all estuaries. For the river-dominated estuaries, the change in river discharge has much more effect, but how much effect is determined by the individual estuary characteristics like the geometry and yearly averaged river discharge, which determines the countering of the tidal wave. So, the differences in river-dominated systems are magnified compared to the tide-dominated systems when changing the river discharge.

A power law relation between the salt intrusion length and river discharge ($L^{HWS} = Q_r^{-\beta_L}$) has been constructed successfully from observations in many estuaries (MacCready & Geyer, 2010). For a static morphology, ranges for β_L have been found between one-seventh (≈ 0.143) and 1, which coincides with our data where β_L ranges from 0.148 for the Ord to 0.684 for the Danube. For example, we found a value for β_L of 0.487 for the Yangtze estuary, where Cai et al. (2015) found a value of 0.43 which is very close. Gong and Shen (2011) came up with a power of 0.49 for the Pearl river, where we found a power of 0.481. For the Hudson, Abood (1974) found that $L_s = Q_r^{-1/3}$ during low river flows and $L_s = Q_r^{-1}$ during high river flows (Monismith et al., 2002). This indicates that for higher river flows, so when the river becomes more important or dominant, β_L becomes higher. This corresponds to the results of our model on the short term, where river-dominated systems often have higher values for β_L than tide-dominated systems. No previous study on this was found where the morphology was dynamic, therefore it is difficult to compare our results on the long term with previous studies. However, the trends in the results can be explained by the interactions between three different processes: 1) the counteracting effect of river discharge on the salt intrusion, 2) the differences in convergence between estuaries, where more convergence makes it easier for the tide to enter the estuary without a large dampening of the tide, and 3) the reduced friction with the bed due to a wider and deeper estuary for increasing river discharge.

River discharge increases or decreases might have large consequences on the salt intrusion and thereby on the estuarine environments and communities. In section 2.3 of the theoretical background, we mentioned some rivers with increasing and decreasing river discharge trends. For example, the Yellow river, Nile and Fraser showed decreasing river discharge trends, while the Mississippi and Orinoco rivers showed upward trends in mean annual river discharge (Shi et al., 2019). Following our research, the consequences for river areas with decreasing mean annual river discharge trends will be that the salt intrusion length will increase. Gong and Shen (2011) indicated that the increase in salt intrusion in recent years in the Pearl river has threatened the freshwater supply in the surrounding regions. Furthermore, agricultural lands may suffer from salinization. River flow can be regulated to a limited extent by hydropower dams (Räsänen et al., 2017; Eslami et al., 2019). Dams can regulate differences in river discharge over the seasons, however, they are often not able to regulate a structural increase or decrease in mean annual river discharge over many years. Adapting the estuary or river flow to limit the salt intrusion will be difficult. However, when research has been done into this and the (future) salt intrusion is known, the surroundings can be prepared or adapted to it. For example, a change in agriculture towards more saline tolerant crops might be an option and/or constructing a fresh water supply network from freshwater zones upstream towards the salt intruded zone (Yan et al., 2013).

7.3 Future research

As discussed in section 7.1, it might be good to distinguish between relatively straight banked river-dominated systems and more convergent tide-dominated systems during the model calibration for a better mouth width prediction. It is expected that river mouths with little convergence behave like rivers and will have values for the hydraulic geometry parameter β of around 0.5, while the tidally influenced and converging river mouths will have values for β around 0.7. Janssen (2022) already concluded that the parameters α and β have the most effect on the width ratio and the convergence lengths. Our 1D tide-averaged model will be globally applicable, but the predictions might be better when zooming in on a particular kind of system.

Furthermore, letting the bed level adapt by adding the sediment conservation equations used by Janssen (2022) might be interesting for future research. The computation time might increase, but Janssen (2022) already showed that the width and bed profile will evolve towards an equilibrium, which is very promising. Next to that, this might solve the underestimation of the mouth width and convergence. Sedimentation and erosion laws can also be added for the width adjustment, which makes it possible to simulate the effects of changing boundary conditions such as sediment supply (Janssen, 2022). In many rivers with hydropower dams, such as the Mekong, Yellow River, Colorado, Nile and Yangtze, sediment is trapped behind the dam causing sediment deficits in the estuary (Gao et al., 2011; Kondolf et al., 2014; Yang et al., 2015). For the Mekong, sediment trapping is even expected to be around 96%, which means that only 4% of the pre-dam sediment load would be expected to reach the delta (Kondolf et al., 2014). This will affect the morphology and is therefore important to research.

Another effect that will be possible to simulate then, is the effects of dredging or sand mining. Hackney et al. (2020) indicated that current sand extraction rates in the lower Mekong River are far above the sediment input rates, meaning that the bed levels can be lowered sufficiently to induce river bank

instability. They stated that regulation of the sand mining is necessary to reach a sustainable balance between the natural supply of sand and the rate at which sand is removed. Many other estuaries are dredged to make transport by ships possible through the estuary channels (Nichols, 2018). This will, just like the sand mining and dam building, upset the estuarine balance and causes a sediment deficit. After some adaption of the model, it will be possible to simulate a sediment deficit and check the effects on the hydrodynamics, morphology and salt intrusion.

Our numerical model can also be used to simulate other changes in boundary conditions. For example, the effects of climate-related changes such as sea-level rise (SLR) can affect estuarine morphology and the salinity distribution. The research by Götte (2020) suggested that sea level rise will have an even bigger impact on the salt intrusion length than changes in river discharge conditions. Following the sixth IPCC report, the global mean SLR by 2100 might reach between 0.63 m and 1.02 m under high greenhouse gas emissions scenarios, compared to 1995-2014 (IPCC, 2021). Due to SLR, estuaries might shift towards more marine-influenced systems with higher water levels, less friction and higher salt intrusion lengths (Chen et al., 2015; Mulligan et al., 2019; Leuven et al., 2021). With our model, it is possible to simulate this and make predictions of the hydrodynamics and morphology of estuaries in the future.

8 Conclusion

In conclusion, a changing river discharge affects the salt intrusion in (morphodynamic) estuaries. Generally, the salt intrusion length increases for smaller river discharges via a power-law relation of the form $L_s = Q_r^{-\beta_L}$. This is due to the decreased friction between the river and tides and therefore decreased counteracting effect of the river. On the short term, the morphology will stay constant, while on the long term, a decrease in river discharge results in narrowing of the estuary and vice versa. Narrowing of the estuary causes the salt intrusion length to decrease on the longer term, although the salt intrusion length stays longer than the initial salt intrusion length for the mean annual river discharge.

Differences in salt intrusion response were found between tide-dominated systems, mixed systems and river-dominated systems. Tide-dominated estuaries have a small river discharge influence on the salt intrusion length on both the short term and the long term, due to small fluvial discharges compared to tidal discharges. The differences in salt intrusion length between the short term and long term are small, due to a small width change. For mixed systems, the river discharge has a large influence on the salt intrusion on both the short term and the long term, due to the counteracting effect of the river discharge on the tides in combination with a relatively large convergence of the estuary mouth. The convergence of the estuary width makes it easier for the tide to enter the estuary without a large dampening due to friction. River-dominated systems also have a large river discharge influence on the salt intrusion length on the short term. However, on the long term, the influence of the river discharge on the salt intrusion is smaller. Since the mouth width of the almost straight channel has extensively narrowed due to a decrease in river discharge, the tide can barely enter the estuary anymore which reduces the income of salt water.

This 1D tide-averaged model shows great potential for more research to gain insight into the long term evolution of salt intrusion and width profiles of estuaries. The width prediction method is globally applicable and can easily be improved when interested in typical kind of systems. When combining our model with the model of Janssen (2022), it might be possible to let the bed level adapt as well to see what will happen with the salt intrusion. Furthermore, the model can be used to predict the effects of sea-level rise or decreasing sediment supply on the estuarine morphology.

References

- Abood, K. A. (1974). Circulation in the Hudson estuary. *Annals of the New York Academy of Sciences*, 250(1), 39–111. <https://doi.org/10.1111/j.1749-6632.1974.tb43895.x>
- Ardón, M., Morse, J. L., Colman, B. P., & Bernhardt, E. S. (2013). Drought-induced saltwater incursion leads to increased wetland nitrogen export. *Global Change Biology*, 19(10), 2976–2985. <https://doi.org/10.1111/gcb.12287>
- Bianchi, T. S. (2013). Estuaries: Where the river meets the sea. *Nature Education Knowledge*, 4, 12.
- Bless, A. E., Colin, F., Crabit, A., Devaux, N., Philippon, O., & Follain, S. (2018). Landscape evolution and agricultural land salinization in coastal area: A conceptual model. *Science of The Total Environment*, 625, 647–656. <https://doi.org/10.1016/j.scitotenv.2017.12.083>
- Boerema, A., & Meire, P. (2017). Management for estuarine ecosystem services: A review. *Ecological Engineering*, 98, 172–182. <https://doi.org/10.1016/j.ecoleng.2016.10.051>
- Bolla Pittaluga, M., Tambroni, N., Canestrelli, A., Slingerland, R., Lanzoni, S., & Seminara, G. (2015). Where river and tide meet: The morphodynamic equilibrium of alluvial estuaries. *Journal of Geophysical Research: Earth Surface*, 120(1), 75–94. <https://doi.org/10.1002/2014JF003233>
- Braat, L., van Kessel, T., Leuven, J. R. F. W., & Kleinhans, M. G. (2017). Effects of mud supply on large-scale estuary morphology and development over centuries to millennia. *Earth Surface Dynamics*, 5(4), 617–652. <https://doi.org/10.5194/esurf-5-617-2017>
- Buschman, F. A. (2011). *Flow and sediment transport in an Indonesian tidal network*. Utrecht University.
- Cai, H., Savenije, H. H. G., & Toffolon, M. (2012). A new analytical framework for assessing the effect of sea-level rise and dredging on tidal damping in estuaries. *Journal of Geophysical Research*, 117(C09023). <https://doi.org/10.1029/2012JC008000>
- Cai, H., Savenije, H. H., Zuo, S., Jiang, C., & Chua, V. P. (2015). A predictive model for salt intrusion in estuaries applied to the yangtze estuary. *Journal of Hydrology*, 529, 1336–1349. <https://doi.org/10.1016/j.jhydrol.2015.08.050>
- Cañedo-Argüelles, M., Kefford, B. J., Piscart, C., Prat, N., Schäfer, R. B., & Schulz, C.-J. (2013). Salinisation of rivers: An urgent ecological issue. *Environmental Pollution*, 173, 157–167. <https://doi.org/10.1016/j.envpol.2012.10.011>
- Canestrelli, A., Lanzoni, S., & Fagherazzi, S. (2014). One-dimensional numerical modeling of the long-term morphodynamic evolution of a tidally-dominated estuary: The Lower Fly River (Papua New Guinea). *Sedimentary Geology*, 301, 107–119. <https://doi.org/10.1016/j.sedgeo.2013.06.009>
- Cao, S., & Knight, D. W. (1996). Regime theory of alluvial channels based upon the concepts of stream power and probability. *Water, Maritime and Energy*, 118, 160–167. <https://doi.org/10.1680/iwtme.1996.28683>
- Chen, W.-B., Liu, W.-C., & Hsu, M.-H. (2015). Modeling assessment of a saltwater intrusion and a transport time scale response to sea-level rise in a tidal estuary. *Environmental Fluid Mechanics*, 15, 491–514. <https://doi.org/10.1007/s10652-014-9367-y>
- Cohen, S., Kettner, A. J., Syvitski, J. P. M., & Fekete, B. M. (2013). WBMsed, a distributed global-scale riverine sediment flux model: Model description and validation. *Computers & Geosciences*, 53, 80–93. <https://doi.org/10.1016/j.cageo.2011.08.011>
- Cunge, J. A., Holly, F. M., & Verwey, A. (1980). *Practical aspects of computational river hydraulics*. London: Pitman.
- Dalrymple, R. W., Zaitlin, B. A., & Boyd, R. (1992). Estuarine facies models; conceptual basis and stratigraphic implications. *Journal of Sedimentary Research*, 62, 1130–1146. <https://doi.org/10.1306/D4267A69-2B26-11D7-8648000102C1865D>
- Davidson, N. C., Laffoley, D. d., Doody, J. P., Way, L. S., Gordon, J., Key, R., Drake, C. M., Pienkowski, M. W., Mitchell, R., & Duff, K. (1991). *Nature conservation and estuaries in Great Britain*. Peterborough, Nature Conservancy Council.
- Davies, G., & Woodroffe, C. D. (2010). Tidal estuary width convergence: Theory and form in North Australian estuaries. *Earth Surface Processes and Landforms*, 35(7), 737–749. <https://doi.org/10.1002/esp.1864>
- Davies, J. L. (1964). A morphogenic approach to world shorelines. *Zeitschrift für Geomorphologie*, 8, 127–142. <https://doi.org/10.1127/zfg/mortensen/8/1964/127>
- Davis Jr, R. A., & Dalrymple, R. W. (2011). *Principles of tidal sedimentology*. Springer Science & Business Media.
- Dronkers, J. (2017). Convergence of estuarine channels. *Continental Shelf Research*, 144, 120–133. <https://doi.org/10.1016/j.csr.2017.06.012>

- Dronkers, J. (n.d.). Physics of coastal systems, lecture course Utrecht University.
- Egbert, G. D., & Erofeeva, S. Y. (2002). Efficient inverse modeling of barotropic ocean tides. *Journal of Atmospheric and Oceanic Technology*, *19*, 183–204. [https://doi.org/10.1175/1520-0426\(2002\)019<0183:EIMOBO>2.0.CO;2](https://doi.org/10.1175/1520-0426(2002)019<0183:EIMOBO>2.0.CO;2)
- Eslami, S., Hoekstra, P., Nguyen Trung, N., Ahmed Kantoush, S., Van Binh, D., Duc Dung, D., Tran Quang, T., & Van der Vegt, M. (2019). Tidal amplification and salt intrusion in the Mekong Delta driven by anthropogenic sediment starvation. *Scientific Reports*, *9*(18746). <https://doi.org/10.1038/s41598-019-55018-9>
- Etemad-Shahidi, A., Parsa, J., & Hajiani, M. (2011). Salinity intrusion length: Comparison of different approaches. *Proceedings of the Institution of Civil Engineers - Maritime Engineering*, *164*(1), 33–42. <https://doi.org/10.1680/maen.2011.164.1.33>
- Farr, T. G., Rosen, P. A., Caro, E., Crippen, R., Duren, R., Hensley, S., Kobrick, M., Paller, M., Rodriguez, E., Roth, L., Seal, D., Shaffer, S., Shimada, J., Umland, J., Werner, M., Oskin, M., Burbank, D., & Alsdorf, D. (2007). The shuttle radar topography mission. *Reviews of Geophysics*, *45*(2). <https://doi.org/10.1029/2005RG000183>
- Friedrichs, C. T., & Aubrey, D. G. (1994). Tidal propagation in strongly convergent channels. *Journal of Geophysical Research: Oceans*, *99*(C2), 3321–3336. <https://doi.org/10.1029/93JC03219>
- Galloway, W. E. (1975). Process framework for describing the morphologic and stratigraphic evolution of deltaic depositional systems (M. Broussard, Ed.). *Deltas: Models for Exploration*, 87–98.
- Gao, P., Mu, X.-M., Wang, F., & Li, R. (2011). Changes in streamflow and sediment discharge and the response to human activities in the middle reaches of the Yellow River. *Hydrology and Earth System Sciences*, *15*(1), 1–10. <https://doi.org/10.5194/hess-15-1-2011>
- Gerten, D., Rost, S., von Bloh, W., & Lucht, W. (2008). Causes of change in 20th century global river discharge. *Hydrology and Land Surface Studies*, *35*. <https://doi.org/10.1029/2008GL035258>
- Geyer, W. R. (2010). Estuarine salinity structure and circulation. In A. Valle-Levinson (Ed.), *Contemporary issues in estuarine physics* (pp. 12–26). Cambridge University Press. <https://doi.org/10.1017/CBO9780511676567.003>
- Gisen, J. I. A., Savenije, H. H. G., & Nijzink, R. C. (2015). Revised predictive equations for salt intrusion modelling in estuaries. *Hydrology and Earth System Sciences*, *19*, 2791–2803. <https://doi.org/10.5194/hess-19-2791-2015>
- Gong, W., & Shen, J. (2011). The response of salt intrusion to changes in river discharge and tidal mixing during the dry season in the modaoemen estuary, china. *Continental Shelf Research*, *31*(7), 769–788. <https://doi.org/10.1016/j.csr.2011.01.011>
- Götte, J. (2020). *Saltwater intrusion in delta regions around the world* (Master's thesis). Utrecht University. Utrecht, the Netherlands.
- Grasso, F., Bismuth, E., & Verney, R. (2021). Unraveling the impacts of meteorological and anthropogenic changes on sediment fluxes along an estuary-sea continuum. *Scientific Reports*, *11*(20230). <https://doi.org/10.1038/s41598-021-99502-7>
- Hackney, C. R., Darby, S. E., Parsons, D. R., Leyland, J., Best, J. L., Aalto, R., Nicholas, A. P., & Houseago, R. C. (2020). River bank instability from unsustainable sand mining in the lower Mekong River. *Nature Sustainability*, *3*, 217–225. <https://doi.org/10.1038/s41893-019-0455-3>
- Haddeland, I., Heinke, J., Biemans, H., Eisner, S., Flörke, M., Hanasaki, N., Konzmann, M., Ludwig, F., Masaki, Y., Schewe, J., Stacke, T., Tessler, Z. D., Wada, Y., & Wisser, D. (2014). Global water resources affected by human interventions and climate change. *Proceedings of the National Academy of Sciences*, *111*(9), 3251–3256. <https://doi.org/10.1073/pnas.1222475110>
- Herbert, E. R., Boon, P., Burgin, A. J., Neubauer, S. C., Franklin, R. B., Ardón, M., Hopfensperger, K. N., Lamers, L. P. M., & Gell, P. (2015). A global perspective on wetland salinization: Ecological consequences of a growing threat to freshwater wetlands. *Ecosphere*, *6*(10), art206. <https://doi.org/10.1890/ES14-00534.1>
- Hey, R. D., & Thorne, C. R. (1986). Stable channels with mobile gravel beds. *Journal of Hydraulic Engineering*, *112*(8), 671–689. [https://doi.org/10.1061/\(ASCE\)0733-9429\(1986\)112:8\(671\)](https://doi.org/10.1061/(ASCE)0733-9429(1986)112:8(671))
- Hoitink, A. J. F., Wang, Z. B., Vermeulen, B., Huismans, Y., & Kästner, K. (2017). Tidal controls on river delta morphology. *Nature Geoscience*, *10*, 637–645. <https://doi.org/10.1038/ngeo3000>
- Hume, T. M., & Herdendorf, C. E. (1988). A geomorphic classification of estuaries and its application to coastal resource management—a New Zealand example. *Ocean and Shoreline Management*, *11*, 249–274. [https://doi.org/10.1016/0951-8312\(88\)90022-7](https://doi.org/10.1016/0951-8312(88)90022-7)
- IPCC. (2021). *Climate change 2021: The physical science basis* (Contribution of Working Group I to the Sixth Assessment Report of the Intergovernmental Panel on Climate Change. V. Masson-

- Delmotte and P. Zhai and A. Pirani and S.L. Connors and C. Péan and S. Berger and N. Caud and Y. Chen and L. Goldfarb and M. I. Gomis and M. Huang and K. Leitzell and E. Lonnoy and J. B. R. Matthews and T. K. Maycock and T. Waterfield and O. Yelekçi and R. Yu and B. Zhou, Ed.) [In Press]. Cambridge University Press.
- Iwantoro, A. P., Van der Vegt, M., & Kleinans, M. G. (2021). Effects of sediment grain size and channel slope on the stability of river bifurcations. *Earth Surface Processes and Landforms*, *46*, 2004–2018. <https://doi.org/10.1002/esp.5141>
- Janssen, M. (2022). *Morphodynamic equilibrium of width and bed level profile of an estuary in response to adjustable channel widths* (Master's thesis). Utrecht University. Utrecht, Netherlands.
- Jeuken, M. C. J. L., Wang, Z. B., Keiller, D., Townend, I., & Liek, G. A. (2003). Morphological response of estuaries to nodal tide variation [paper presented at International Conference on Estuaries and Coasts].
- Kleinans, M. G., Cohen, K. M., Hoekstra, J., & IJmker, J. M. (2011). Evolution of a bifurcation in a meandering river with adjustable channel widths, rhine delta apex, the netherlands. *Earth Surface Processes and Landforms*, *36*(15), 2011–2027. <https://doi.org/10.1002/esp.2222>
- Kondolf, G. M., Rubin, Z. K., & Minear, J. T. (2014). Dams on the Mekong: Cumulative sediment starvation. *Water Resources Research*, *50*(6), 5158–5169. <https://doi.org/10.1002/2013WR014651>
- Lacey, G. (1930). Stable channels in alluvium. *Minutes of the Proceedings of the Institution of Civil Engineers*, *229*, 259–292. <https://doi.org/10.1680/imotp.1930.15592>
- Langbein, W. B. (1963). The hydraulic geometry of a shallow estuary. *Hydrological Sciences Journal*, *8*, 84–94. <https://doi.org/10.1080/02626666309493340>
- Lanzoni, S., & Seminara, G. (2002). Long-term evolution and morphodynamic equilibrium of tidal channels. *Journal of Geophysical Research: Oceans*, *107*, 1–13. <https://doi.org/10.1029/2000JC000468>
- Leopold, L. B., & Maddock, T. (1953). *The hydraulic geometry of stream channels and some physiographic implications* (Vol. 252). US Geological Survey.
- Leuven, J. R. F. W., de Haas, T., Braat, L., & Kleinans, M. G. (2018). Topographic forcing of tidal sandbar patterns for irregular estuary planforms. *Earth Surface Processes and Landforms*, *43*(1), 172–186. <https://doi.org/10.1002/esp.4166>
- Leuven, J. R. F. W., Kleinans, M. G., Weisscher, S. A. H., & Van der Vegt, M. (2016). Tidal sand bar dimensions and shapes in estuaries. *Earth-Science Reviews*, *161*, 204–223. <https://doi.org/10.1016/j.earscirev.2016.08.004>
- Leuven, J. R. F. W., Pierik, H. J., Van der Vegt, M., Bouma, T. J., & Kleinans, M. G. (2019). Sea-level-rise-induced threats depend on the size of tide-influenced estuaries worldwide. *Nature climate change*, *9*, 986–992. <https://doi.org/10.1038/s41558-019-0608-4>
- Leuven, J. R. F. W., Van Keulen, D., Nienhuis, J. H., Canestrelli, A., & Hoitink, A. J. F. (2021). Large-scale scour in response to tidal dominance in estuaries. *Journal of Geophysical Research: Earth Surface*, *126*. <https://doi.org/10.1016/j.csr.2017.06.012>
- Liu, W.-C., Chen, W.-B., Cheng, R. T., Hsu, M.-H., & Kuo, A. Y. (2007). Modeling the influence of river discharge on salt intrusion and residual circulation in danshuei river estuary, taiwan. *Continental Shelf Research*, *27*(7), 900–921. <https://doi.org/10.1016/j.csr.2006.12.005>
- MacCready, P., & Geyer, W. R. (2010). Advances in estuarine physics. *Annual Review of Marine Science*, *2*(1), 35–58. <https://doi.org/10.1146/annurev-marine-120308-081015>
- Mikhailov, V. N. (1970). Hydrologic-morphometric characteristics of delta branches. *Studies and Reports in Hydrology*, *9*, 146–158. <https://iahs.info/uploads/dms/3364.146-158-90-Mikhailov.pdf>
- Miori, S., Repetto, R., & Tubino, M. (2006). A one-dimensional model of bifurcations in gravel bed channels with erodible banks. *Water Resources Research*, *42*(11). <https://doi.org/10.1029/2006WR004863>
- Monismith, S. G., Kimmerer, W., Burau, J. R., & Stacey, M. T. (2002). Structure and flow-induced variability of the subtidal salinity field in Northern San Francisco Bay. *Journal of Physical Oceanography*, *32*(11), 3003–3019. [https://doi.org/10.1175/1520-0485\(2002\)032<3003:SAFIVO>2.0.CO;2](https://doi.org/10.1175/1520-0485(2002)032<3003:SAFIVO>2.0.CO;2)
- Mulligan, R. P., Mallinson, D. J., Clunies, G. J., Rey, A., Culver, S. J., Zaremba, N., Leorri, E., & Mitra, S. (2019). Estuarine responses to long-term changes in inlets, morphology, and sea level rise. *Journal of Geophysical Research: Oceans*, *124*, 9235–9257. <https://doi.org/10.1029/2018JC014732>
- Myrick, R. M., & Leopold, L. B. (1963). *Hydraulic geometry of a small tidal estuary*. US Government Printing Office.
- Nichols, M. M. (2018). Consequences of dredging. In B. Kjerfve (Ed.), *Hydrodynamics of estuaries: Volume II estuarine case studies*. CRC Press.

- Nienhuis, J. H., Ashton, A. D., Edmonds, D. A., Hoitink, A. J. F., Kettner, A. J., Rowland, J. C., & Törnqvist, T. E. (2020). Global-scale human impact on delta morphology has led to net land area gain. *Nature*, *577*, 514–518. <https://doi.org/10.1038/s41586-019-1905-9>
- Nienhuis, J. H., Hoitink, A. J. F., & Törnqvist, T. E. (2018). Future change to tide-influenced deltas. *Geophysical Research Letters*, *45*, 3499–3507. <https://doi.org/10.1029/2018GL077638>
- Noe, G. B., Krauss, K. W., Lockaby, B. G., H., C. W., & R., H. C. (2013). The effect of increasing salinity and forest mortality on soil nitrogen and phosphorus mineralization in tidal freshwater forested wetlands. *Biogeochemistry*, *114*, 225–244. <https://doi.org/10.1007/s10533-012-9805-1>
- Nohara, D., Kitoh, A., Hosaka, M., & Oki, T. (2006). Impact of climate change on river discharge projected by multimodel ensemble. *Journal of Hydrometeorology*, *7*, 1076–1089. <https://doi.org/10.1175/JHM531.1>
- Parsa, J., & Etemad-Shahidi, A. (2010). Prediction of tidal excursion length in estuaries due to the environmental changes. *International Journal of Environment Science and Technology*, *7*(4), 675–686. <https://doi.org/10.1007/BF03326177>
- Perillo, G. M. (1995). *Geomorphology and sedimentology of estuaries*. Elsevier.
- Pidwirny, M. (2006). *Ocean tides* (2nd ed.). Retrieved February 6, 2022, from www.physicalgeography.net/fundamentals/8r.html
- Pritchard, D. W. (1967). What is an estuary: Physical viewpoint. In G. Lauff (Ed.), *Estuaries*. American Association for the Advancement of Science.
- Prudhomme, C., Giuntoli, I., Robinson, E. L., Clark, D. B., Arnell, N. W., Dankers, R., Fekete, B. M., Franssen, W., Gerten, D., Gosling, S. N., Hagemann, S., Hannah, D. M., Kim, H., Masaki, Y., Satoh, Y., Stacke, T., Wada, Y., & Wisser, D. (2014). Hydrological droughts in the 21st century, hotspots and uncertainties from a global multimodel ensemble experiment. *Proceedings of the National Academy of Sciences*, *111*(9), 3262–3267. <https://doi.org/10.1073/pnas.1222473110>
- Pugh, D., & Woodworth, P. (2014). Introduction. *Sea-level science: Understanding tides, surges, tsunamis and mean sea-level changes* (pp. 1–16). Cambridge University Press. <https://doi.org/10.1017/CBO9781139235778.004>
- Räsänen, T. A., Someth, P., Lauri, H., Koponen, J., Sarkkula, J., & Kummur, M. (2017). Observed river discharge changes due to hydropower operations in the upper mekong basin. *Journal of Hydrology*, *545*, 28–41. <https://doi.org/10.1016/j.jhydrol.2016.12.023>
- Retsinis, E., & Papanicolaou, P. (2020). Numerical and experimental study of classical hydraulic jump. *Water*, *12*, 1766. <https://doi.org/10.3390/w12061766>
- Rinaldo, A., Fagherazzi, S., Lanzoni, S., Marani, M., & Dietrich, W. E. (1999). Tidal networks: 3. landscape-forming discharges and studies in empirical geomorphic relationships. *Water Resources Research*, *35*(12), 3919–3929. <https://doi.org/10.1029/1999WR900238>
- Rosendahl Appelquist, L., & Halsnæs, K. (2015). The coastal hazard wheel system for coastal multi-hazard assessment & management in a changing climate. *Journal of Coastal Conservation*, *19*. <https://doi.org/10.1007/s11852-015-0379-7>
- Sassi, M. G., Hoitink, A. J. F., de Brye, B., & Deleersnijder, E. (2012). Downstream hydraulic geometry of a tidally influenced river delta. *Journal of Geophysical Research Letters*, *117*, F04022. <https://doi.org/10.1029/2012JF002448>
- Savenije, H. H. G. (1989). Salt intrusion model for high-water slack, low-water slack, and mean tide on spread sheet. *Journal of Hydrology*, *107*, 9–18. [https://doi.org/10.1016/0022-1694\(89\)90046-2](https://doi.org/10.1016/0022-1694(89)90046-2)
- Savenije, H. H. G. (1993). Predictive model for salt intrusion in estuaries. *Journal of Hydrology*, *148*, 203–218. [https://doi.org/10.1016/0022-1694\(93\)90260-G](https://doi.org/10.1016/0022-1694(93)90260-G)
- Savenije, H. H. G. (2001). A simple analytical expression to describe tidal damping or amplification. *Journal of Hydrology*, *243*(3), 205–215. [https://doi.org/10.1016/S0022-1694\(00\)00414-5](https://doi.org/10.1016/S0022-1694(00)00414-5)
- Savenije, H. H. G. (2012). *Salinity and tides in alluvial estuaries* (2nd ed.). salinityandtides.com
- Saysel, A. K., & Barlas, Y. (2001). A dynamic model of salinization on irrigated lands. *Ecological Modelling*, *139*(2), 177–199. [https://doi.org/10.1016/S0304-3800\(01\)00242-3](https://doi.org/10.1016/S0304-3800(01)00242-3)
- Scanes, P., Ferguson, A., & Potts, J. (2017). Estuary form and function: Implications for palaeoecological studies. *Applications of paleoenvironmental techniques in estuarine studies* (pp. 9–44). Springer Netherlands. https://doi.org/10.1007/978-94-024-0990-1_2
- Shi, X., Qin, T., Nie, H., Weng, B., & He, S. (2019). Changes in major global river discharges directed into the ocean. *International Journal of Environmental Research and Public Health*, *16*(1469). <https://doi.org/10.3390/ijerph16081469>
- Syvitski, J. P. M., & Saito, Y. (2007). Morphodynamics of deltas under the influence of humans. *Global and Planetary Change*, *57*, 261–282. <https://doi.org/10.1016/j.gloplacha.2006.12.001>

- Teh, S. Y., & Koh, H. L. (2016). Climate change and soil salinization: Impact on agriculture, water and food security. *International Journal of Agriculture, Forestry and Plantation*, 2.
- Todeschini, I., Toffolon, M., & Tubino, M. (2008). Long-term morphological evolution of funnel-shape tide-dominated estuaries. *Journal of Geophysical Research: Oceans*, 113(C5). <https://doi.org/10.1029/2007JC004094>
- Townend, I. (2012). The estimation of estuary dimensions using a simplified form model and the exogenous controls. *Earth Surface Processes and Landforms*, 37(15), 1573–1583. <https://doi.org/10.1002/esp.3256>
- Uncles, R. J., & Stephens, J. A. (1996). Salt intrusion in the Tweed estuary. *Estuarine, Coastal and Shelf Science*, 43(3), 271–293. <https://doi.org/10.1006/ecss.1996.0070>
- van Vliet, M. T. H., Franssen, W. H. P., Yearsley, J. R., Ludwig, F., Haddeland, I., Lettenmaier, D. P., & Kabat, P. (2013). Global river discharge and water temperature under climate change. *Global Environmental Change*, 23(2), 450–464. <https://doi.org/10.1016/j.gloenvcha.2012.11.002>
- van Leussen, W. (1999). The variability of settling velocities of suspended fine-grained sediment in the Ems estuary. *Journal of Sea Research*, 41, 109–118. [https://doi.org/10.1016/S1385-1101\(98\)00046-X](https://doi.org/10.1016/S1385-1101(98)00046-X)
- van Rijn, L. C. (2011). Analytical and numerical analysis of tides and salinities in estuaries; part I: Tidal wave propagation in convergent estuaries. *Ocean Dynamics*, 61, 1719–1741. <https://doi.org/10.1007/s10236-011-0453-0>
- Wang, W., & Lu, Y. (2018). Analysis of the Mean Absolute Error (MAE) and the Root Mean Square Error (RMSE) in assessing rounding model. *IOP Conference Series: Materials Science and Engineering*, 324, 012049. <https://doi.org/10.1088/1757-899X/324/1/012049>
- Wolanski, E., & Elliot, M. (2015). *Estuarine ecohydrology: An introduction* (2nd ed.). Elsevier.
- Wolanski, E., Moore, K., Spagnol, S., D'Adamo, N., & Pattiaratchi, C. (2001). Rapid, human-induced siltation of the macro-tidal ord river estuary, western australia. *Estuarine, Coastal and Shelf Science*, 53(5), 717–732. <https://doi.org/10.1006/ecss.2001.0799>
- Xu, F., Coco, G., Townend, I., Guo, L., He, Q., Zhao, K., & Zhou, Z. (2021). Rationalizing the differences among hydraulic relationships using a process-based model. *Water Resources Research*, 57(8), e2020WR029430. <https://doi.org/10.1029/2020WR029430>
- Yan, K., Shao, H., Shao, C., Chen, P., Zhao, S., Brestic, M., & Chen, X. (2013). Physiological adaptive mechanisms of plants grown in saline soil and implications for sustainable saline agriculture in coastal zone. *Acta Physiologiae Plantarum*, 35, 2867–2878. <https://doi.org/10.1007/s11738-013-1325-7>
- Yang, S. L., Xu, K. H., Milliman, J. D., Yang, H. F., & Wu, C. S. (2015). Decline of Yangtze River water and sediment discharge: Impact from natural and anthropogenic changes. *Scientific Reports*, 5(12581). <https://doi.org/10.1038/srep12581>
- Zhao, J., Guo, L., He, Q., Wang, Z. B., van Maren, D., & Wang, X. (2018). An analysis on half century morphological changes in the Changjiang estuary: Spatial variability under natural processes and human intervention. *Journal of Marine Systems*, 181, 25–36. <https://doi.org/10.1016/j.jmarsys.2018.01.007>
- Zhou, Z., Coco, G., Townend, I., Olabarrieta, M., van der Wegen, M., Gong, Z., D'Alpaos, A., Gao, S., Jaffe, B. E., Gelfenbaum, G., He, Q., Wang, Y., Lanzoni, S., Wang, Z., Winterwerp, H., & Zhang, C. (2017). Is “morphodynamic equilibrium” an oxymoron? *Earth-Science Reviews*, 165, 257–267. <https://doi.org/10.1016/j.earscirev.2016.12.002>

Appendices

A Notation

Table 2: Symbols and units used in this report.

Symbol	Description	Unit
a_t	Tidal water level amplitude	m
A	Channel cross-sectional area	m ²
A_e	Surface area of the estuary	m ²
A_m	Channel cross-sectional area at estuary mouth	m ²
B	Channel width	m
B_{ave}	Channel width for mean annual river discharge	m
B_e	Equilibrium channel width	m
B_m	Channel width at the mouth	m
B_r	Channel width at the river	m
C_d	Drag coefficient	—
E	Tidal excursion length	m
E_m	Tidal excursion length at the mouth	m
Fr	Froude number	—
g	Gravitational acceleration	m s ⁻²
h	Channel depth	m
h_m	Channel depth at the mouth	m
h_r	Channel depth at the river	m
H	Tidal range	m
H_m	Tidal range at the mouth	m
I	Tide-dominance ratio based on water discharge	—
K	Van der Burgh's coefficient	—
L_a	Cross-sectional area convergence length	m
L_b	Width convergence length	m
L_e	Estuary length	m
L_s	Salt intrusion length	m
L_t	Tidal length	m
L^{HWS}	Salt intrusion length at high water slack	m
L_{ave}^{HWS}	Salt intrusion length at HWS for mean annual river discharge	m
L^{LWS}	Salt intrusion length at low water slack	m
L^{TA}	Tidal average salt intrusion length	m
n	Number of distributary channels	—
N	Number of prediction pairs	—
P	Tidal prism	m ³
P_m	Tidal prism at the mouth	m ³
P_r	Tidal prism at the river	m ³
Q	Discharge	m ³ s ⁻¹
Q_{peak}	Discharge peak	m ³ s ⁻¹
Q_r	River discharge	m ³ s ⁻¹
$Q_{r,ave}$	Mean annual river discharge	m ³ s ⁻¹
Q_t	Tidal discharge	m ³ s ⁻¹
$Q_{t,ave}$	Tidal discharge belonging to mean annual river discharge	m ³ s ⁻¹
$Q_{t,max}$	Maximum tidal discharge amplitude	m ³ s ⁻¹
Q_w	Wave discharge	m ³ s ⁻¹
$RMSE$	Root mean square error	—
R_r	Fluvial dominance ratio based on sediment discharge	—
S	Channel slope	—
t	Time	s
T	Tidal period	s
T_r	Tide-dominance ratio based on sediment discharge	—
T_w	Width adjustment timescale	s

\bar{u}	Mean flow velocity	m s^{-1}
U	Non-dimensional velocity scale	—
W_p	Wetted perimeter	m
x	Distance	m
x_b	Distance of mouth to furthest point upstream where $B > B_r$	m
\hat{y}_n	Predicted value	Same as input
y_n	Observed value	Same as input
Z	Water level	m
Z_m	Water level at the mouth	m
a	Coefficient for empirical relation river width	—
b	Exponent for empirical relation river width	—
α	Coefficient for empirical relation estuary width	—
α_A	Coefficient for empirical relation cross-sectional area	—
α_m	Mixing coefficient at the estuary mouth	—
β	Exponent for empirical relation estuary width	—
β_A	Exponent for empirical relation cross-sectional area	—
β_B	Exponent for relation width - river discharge	—
β_L	Exponent for relation salt intrusion length - river discharge	—
β_m	Positive coefficient in salt intrusion prediction	—
η	Bed elevation	m
ϕ	Tidal phase	rad
v_m	Tidal velocity amplitude at the mouth	m s^{-1}

B Estuary data

Table 3: Estuary data by Nienhuis et al. (2018) and Gisen et al. (2015) used in this research.

No.	Estuary	Q_r ($\text{m}^3 \text{s}^{-1}$)	h_m (m)	S (-)	H_m (m)	T (h)	B_r (m)	B_m (m)	L^{HWS} (km)
Data set by Nienhuis et al. (2018)									
1	Amazon	198,676	23.3	2.0E-5	6.0	12	6000	30600	
2	Arno	57	2.0	3.4E-4	0.7	12	80	125	
3	Brazos	189	2.9	1.3E-4	0.7	24	150	230	
4	Ceyan	222	3.0	2.4E-4	0.7	12	111	150	
5	Chao Phraya	963	4.7	2.0E-5	2.0	24	266	866	
6	Colorado (MX)	694	4.3	3.6E-5	5.0	12	120	4596	
7	Colorado (TX)	76	2.2	1.3E-4	0.7	24	107	131	
8	St George, Danube	1500	5.4	7.8E-5	0.1	12	400	470	
9	Ebro	600	4.1	1.9E-4	0.2	24	235	315	
10	Eel	235	3.1	7.2E-4	3.0	12	103	300	
11	Fly	5700	8.0	1.5E-5	4.0	12	500	17500	
12	Fraser	3560	7.0	5.8E-5	4.5	12	300	1626	
13	Ganges/Brahmaputra	31,000	13.4	3.5E-5	3.6	12	7500	17321	
14	Godavari	2650	6.4	1.7E-4	1.5	12	2000	2021	
15	Homathko	253	3.2	2.1E-3	3.6	12	150	283	
16	Huanghe	1480	5.4	8.0E-5	0.8	12	550	800	
17	Indus	3171	6.7	5.2E-5	5.0	12	613	2500	
18	Irrawaddy	13,558	10.4	4.0E-5	4.2	12	1300	8500	
19	Klamath	473	3.8	7.5E-4	3.0	12	170	240	
20	Klinaklini	330	3.4	1.1E-3	4.0	12	300	424	
21	Kolyma	3784	7.1	2.5E-5	1.0	12	2500	6351	
22	Krishna	1890	5.8	1.1E-4	1.5	12	800	1212	
23	Limpopo	835	4.5	1.0E-4	1.2	12	405	550	
24	Magdalena	7530	8.7	9.8E-5	1.0	24	900	910	
25	Mahanadi	2112	6.0	5.2E-5	3.5	12	1000	1697	
26	Mekong	17,345	11.2	2.8E-5	2.6	24	2700	5103	
27	Mississippi	15,452	10.8	2.1E-5	0.4	24	1000	1118	
28	Niger	6130	8.2	8.3E-5	3.0	12	1400	2907	
29	Nile	3484	6.9	4.5E-5	0.4	12	382	463	
30	Orange	442	3.7	2.2E-4	1.5	12	210	228	
31	Orinoco	34,500	13.8	2.1E-5	1.9	12	3000	8165	
32	Parana	14,506	10.6	3.2E-5	0.8	12	1500	1671	
33	Pechora	4099	7.3	4.0E-5	3.0	12	1500	2367	
34	Pescara	29	1.6	5.2E-4	0.6	12	37	38	
35	Po	1525	5.4	6.5E-5	0.7	12	383	485	
36	Rhone	1700	5.6	1.6E-4	0.5	12	400	636	
37	Song Hong (Red River)	3784	7.1	5.1E-5	3.5	24	600	1455	
38	Squamish	250	3.1	7.8E-4	3.0	12	110	200	
39	Tigris-Euphrates	1500	5.4	4.0E-5	3.0	12	235	778	
40	Var	41	1.8	3.8E-3	0.5	12	75	80	
41	Vistula (Wisla)	1050	4.8	1.3E-4	1.0	24	400	472	
42	Waipaoa	41	1.8	1.3E-3	1.2	12	110	120	
43	Yangtze	28,278	13.0	3.1E-5	4.5	12	1700	13500	
44	Zhujiang (Pearl)	8199	9.0	1.3E-5	5.0	12	800	8660	
45	Pericumá	115	2.5	5.0E-5	7.4	12	100	1500	
46	Maracana	238	3.1	5.0E-5	6.0	12	180	2058	
47	Marapanim	186	2.9	5.0E-5	6.1	12	189	2954	
48	Cacipore	514	3.9	5.0E-5	4.0	12	200	4000	
49	Suriname	440	3.7	1.0E-4	2.8	12	557	2000	
50	Demerara	300	3.3	1.0E-4	3.1	12	200	900	
51	Sungai Merauke	330	3.4	6.0E-5	3.1	12	90	900	
52	Santa Lucia	2700	6.4	2.0E-4	0.7	12	447	707	
53	Mahi	380	3.6	4.0E-5	10.9	12	342	11505	
54	Narmada	1447	5.3	5.0E-5	12.4	12	512	4950	
55	Tapi	550	4.0	1.0E-4	6.3	12	614	1980	

No.	Estuary	Q_r ($\text{m}^3 \text{s}^{-1}$)	h_m (m)	S (-)	H_m (m)	T (h)	B_r (m)	B_m (m)	L^{HWS} (km)
56	Purna	120	2.5	2.0E-4	6.5	12	98	1126	
57	Hooghly	16,000	10.9	4.0E-5	3.8	12	1000	12728	
58	Kumbe	144	2.7	1.0E-4	3.8	12	96	330	
59	Yangon/Bago	3887	7.2	2.6E-5	4.1	12	800	6694	
60	Bilin	1490	5.4	1.5E-4	4.8	12	245	3200	
61	Thanlyin	4978	7.7	2.0E-5	4.6	12	1300	7778	
62	Tanintharyi	1000	4.8	2.0E-5	3.5	12	290	3184	
63	Sungai Rokan	727	4.3	4.0E-5	4.8	12	200	7566	
64	Sokyosen	1500	5.4	1.0E-4	10.9	12	236	3200	
65	Taeryong	700	4.3	9.0E-5	6.7	12	435	2500	
66	Yoneshiro	250	3.1	1.0E-4	0.3	12	160	450	
67	Wai Bian	208	3.0	1.2E-4	6.3	12	114	2500	
68	Weser	288	3.3	5.0E-5	3.4	12	150	1500	
69	Thames	65	2.1	2.9E-5	7.5	12	70	6618	
70	Ombrone	31	1.7	4.0E-4	0.4	12	73	116	
71	Tibre	70	2.1	3.0E-4	0.4	12	136	162	
72	Ord	110	2.5	1.0E-4	8.0	12	150	2828	

Data set by Gisen et al. (2015)

73	Kurau	50	5.2	1.5E-4	2.0	12	20	600	17
74	Perak	316	4.5	1.0E-4	2.5	12	130	9670	29
75	Bernam	42	3.5	1.0E-4	2.9	12	45	6180	58
76	Selangor	41	3.6	1.5E-4	4.0	12	35	915	22
77	Muar	35	5.6	1.8E-4	2.0	12	55	823	51
78	Endau	54	6.5	4.4E-4	1.9	12	72	400	29
79	Maputo	120	4.1	1.7E-4	3.3	12	100	9000	27
80	Thames	40	13.9	8.9E-5	5.3	12	50	6700	100
81	Corantijn	220	5.4	5.3E-5	1.6	12	400	30000	87
82	Sinnamary	168	2.4	6.2E-4	2.6	12	95	916	10
83	Mae Klong	60	4.6	1.1E-4	1.5	12	150	250	32
84	Lalang	120	8.0	5.1E-5	2.6	24	130	360	34
85	Limpopo	150	6.3	7.9E-5	1.1	12	90	405	27
86	Tha Chin	40	5.6	4.7E-5	2.6	12	45	3600	51
87	Chao Phya	180	6.5	3.8E-5	2.5	24	200	1950	26
88	Edisto	25	4.1	9.7E-5	2.3	12	60	1460	44
89	Elbe	200	9.3	5.4E-5	3.0	12	350	2880	94
90	Pangani	15	3.2	2.3E-4	4.2	12	35	543	29
91	Rembau Linggi	26	4.6	1.2E-3	2.0	12	25	488	20
92	Landak	10	8.7	7.3E-5	1.6	24	100	230	36
93	Delaware	120	6.8	5.4E-5	1.7	12	120	37655	147
94	Westerschelde	220	9.4	4.6E-5	4.0	12	50	16000	124
95	Pungue	262	2.8	9.4E-5	6.2	12	50	5200	50
96	Incomati	4	2.8	1.7E-4	1.4	12	22	4500	53
97	Solo	50	9.2	1.1E-4	0.8	24	95	225	29
98	Ems	10	3.8	8.7E-5	3.6	12	55	31623	83
99	Tejo	149	5.0	9.4E-5	1.9	12	180	20000	50
100	Rompin	20	6.1	8.1E-4	1.7	12	50	615	43
101	Ulu Sedili Besar	8	4.7	1.4E-4	1.1	12	35	550	28

C Testing the model hydrodynamics

Methods

The hydrodynamics of the model used in this research, the 1D tide-averaged numerical estuary model, are tested by comparing the tidal prism output with the tidal prism output of Nienhuis et al. (2018). Nienhuis et al. (2018) introduced a theory and model to predict the magnitude of downstream channel widening of tide-influenced deltas. It includes two important assumptions: the convergent estuary shape is described by a trapezoidal width profile as illustrated in figure 25, and the water levels rise and fall equally over the estuary, meaning that there is no tidal wave propagation. Just as in our 1D tide-averaged model, the tidal amplitude is assumed to be constant. These assumptions result in the fact that the tidal prism P (m^3) can be related to the channel surface area of the tidally influenced reach times the tidal range by:

$$P = 2a_t A_e = 2a_t \frac{1}{2} (B_m + B_r) L_e \quad (44)$$

with a_t is the offshore tidal amplitude (m), A_e is the surface area of the estuary (m^2), and L_e is the estuary length (m). For the calculation of this tidal prism, the measured mouth width and river width are inserted, while the estuary length is equal to the depth divided by the slope: $L_e = h/S$.

To test the hydrodynamics of the 1D tide-averaged model, the same trapezoidal width profile (see figure 25) is used and kept constant over time. The bed elevation is also constant over time and calculated by equation 23. The water level z is calculated by the hydrodynamics following equation 22 and differs from the approach of Nienhuis et al. (2018) where the water level goes up and down equally over the estuary. This means that the 1D model includes tidal wave propagation in contrast to the model by Nienhuis et al. (2018). When assuming a simple sinus function for a tidal cycle, the tidal prism in the 1D tide-averaged model can be calculated by:

$$P = \frac{1}{2} \cdot \int_0^T \left| Q_{t,max} \sin \left(\frac{2\pi}{T} t \right) \right| dt \quad (45)$$

with $Q_{t,max}$ is the maximum tidal discharge amplitude ($\text{m}^3 \text{s}^{-1}$), T is the tidal period (s) and t is the time (s). A semi-diurnal or diurnal tide is used depending on the dominant tide for the estuary. The integral is multiplied by 1/2, since the inflow during flood or the outflow during ebb is needed, which includes half of a tidal cycle. The total discharge peak is a combination of the river discharge (assumed constant) and tidal discharge peak: $Q_{peak} = Q_r + Q_{t,max}$. So, the tidal discharge amplitude $Q_{t,max}$ is calculated by the peak discharge minus the river discharge.

In the 1D tide-averaged model, a river part is added which is of the same length as the estuary with a constant width equal to the river width. This is done to prevent the tide from reflecting at the upstream boundary. For some deltas with a high tidal influence, the tidal wave might reach into the river meaning that the tidal prism at the mouth (P_m) also includes a small tidal prism for the river (P_r). Since the interest lies in the tidal prism of the estuary, the tidal prism at the boundary of the river and estuary has to be subtracted: $P = P_m - P_r$. The tidal prism is calculated for the 72 estuaries and compared to the tidal prism by Nienhuis et al. (2018) using a log-log plot. The closer the data points for the individual estuaries lie to the 1:1 line ($x=y$, line of perfect agreement), the better the models agree. Although the mouth width for multiple channel systems is corrected by $n^{-0.5}$, see section 4.2, a distinction is made between one channel systems and multiple channel systems to check whether the hydrodynamics work correctly for both system types.

Results

The comparison between the tidal prism prediction by Nienhuis et al. (2018) and the tidal prism prediction by the 1D tide-averaged model, resulted in the plot shown in figure 26. For many estuaries, the tidal prism predicted by the 1D tide-averaged model is smaller than the tidal prism predicted by Nienhuis et al. (2018). This can be explained by the difference in tidal wave propagation. Nienhuis et al. (2018) assumes that water levels go up and down equally over the whole estuary, meaning that every position in the estuary experiences high water or low water at the same time. In reality, tidal waves propagate

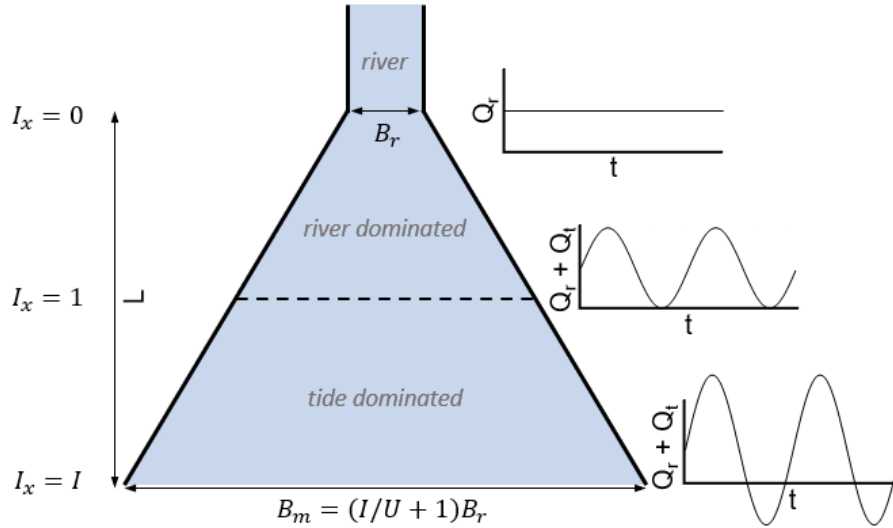


Figure 25: Trapezoidal width profile (Nienhuis et al., 2018).

through the estuary, whereby water levels are not equal over the estuary (Savenije, 2012). For example, water levels at the mouth can already go down while the water levels upstream are still rising. This means that water levels in the whole estuary will never be high or low at the same time, which causes the tidal prism to be lower. The 1D tide-averaged model includes wave propagation, so in this case this model probably gives a better prediction of the tidal prism than the model by Nienhuis et al. (2018).

When plotting the ratio of the tidal prism by Nienhuis et al. (2018) over the tidal prism by the 1D tide-averaged model against the estuary length (L_e) over the tidal wavelength ($L_t = T\sqrt{gh}$, van Rijn (2011)), it becomes clear that this effect is larger for larger estuaries, see figure 27. This also makes sense, since a wave can propagate further in a larger estuary. Since the one channel systems are often smaller, the tidal prism for one channel systems is generally closer to the tidal prism by Nienhuis et al. (2018) than the tidal prism for multiple channel systems. When the tidal wave is amplified due to the convergence of the estuary in combination with a very short estuary, it might be that the tidal prism becomes larger than the tidal prism calculated by Nienhuis et al. (2018) (Leuven et al., 2021). The differences in tidal prism can be explained, meaning that the hydrodynamics can be validated.

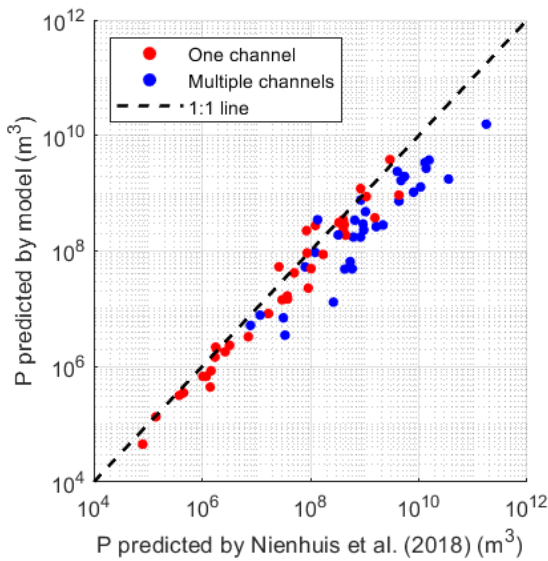


Figure 26: Tidal prism comparison between the 1D tide-averaged model and the model by Nienhuis et al. (2018)

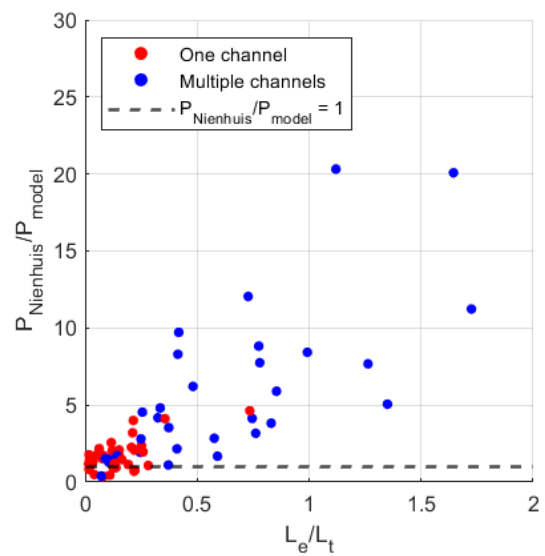


Figure 27: Tidal prism ratio against estuary length over tidal wavelength

D Predictive equations of Gisen et al. (2015)

The predictive equations for the salt intrusion length by Savenije (1993) were revised and improved by Gisen et al. (2015). Where Savenije (1993) used 45 salt intrusion measurements in 15 estuaries to establish the empirical predictive equations, Gisen et al. (2015) expanded the data set to 89 salinity profiles in 30 different estuaries. In this appendix section, the method of Gisen et al. (2015) is given and it is explained why we chose to use the simpler equations of Savenije (1993).

In the research of Gisen et al. (2015) the location of the downstream boundary is not fixed at the estuary mouth, but at an inflection point x_1 , which is the point where the estuary changes from wave-dominated to tide-dominated geometry. This was done to eliminate the difficulty of determining the exact location of the estuary mouth, to reduce the effect of wind and waves and to eliminate the dilemma of which geometry parameters to use in the predictive equations. Following the results of the multiple regression analysis of Gisen et al. (2015), the new predictive equation for the Van der Burgh's coefficient becomes:

$$K = 151.35 \times 10^{-6} \left(\frac{B_r^{0.30} H_1^{0.13} T^{0.97}}{B_1^{0.30} C^{0.18} v_1^{0.71} L_{b,2}^{0.11} \bar{h}_1^{0.15} r_s^{0.84}} \right) \quad (46)$$

with B_r is the river width (m) and T is the tidal period (s). B_1 , H_1 , v_1 , \bar{h}_1 and $L_{b,2}$ represent the estuary width (m), tidal range (m), tidal velocity amplitude (m s^{-1}), tidally averaged estuary depth (m) and width convergence length (m) at the inflection point. C is the Chézy roughness ($\text{m}^{0.5} \text{s}^{-1}$), which was obtained through calibration using the tidal dynamics solution of Cai et al. (2012). r_s is the storage width ratio, which is defined as the ratio between storage width and stream width.

During this study, 18 dispersion regression equations were obtained from the multiple regression analysis. Substituting the best predictive dispersion equations with the highest R^2 into the salt intrusion length (8) gives

$$L^{HWS} = x_1 + L_{a,2} \ln \left(0.3958 \frac{E_1 v_1 g^{0.21}}{K L_{a,2} u_1 C^{0.42} N_r^{0.57} + 1} \right) + \frac{E_m}{2} \quad (47)$$

with E_m and E_1 are the tidal excursion lengths at the mouth and at the inflection point, u_1 is the driver flow velocity at the inflection point (m s^{-1}) and N_r is the estuarine Richardson number (-) which is the ratio of potential energy of the fresh water to the kinetic energy of the tide:

$$N_r = \frac{\Delta \rho g h Q_r T}{\rho v^2 A E} \quad (48)$$

where $\Delta \rho$ is the density difference over the salt intrusion length (kg m^{-3}) and ρ is the fresh water density (kg m^{-3}).

The tidal excursion length and tidal range at the inflection point can be calculated by:

$$E_1 = E_m \exp(\delta_H x_1) \quad (49)$$

$$H_1 = H_m \exp(\delta_H x_1) \quad (50)$$

with δ_H is the tidal damping factor which also follows from the tidal dynamic simulation of Cai et al. (2012).

The largest difficulty with this salt intrusion prediction method, is that not all data that is necessary is also available. Except for the tidal velocity amplitude v , driver flow velocity u and storage width ratio r_s , all data can be found in the supplement of Gisen et al. (2015). However, such extensive data is not always available for other estuaries, like the ones of the data set by Nienhuis et al. (2018). In the 1D tide-averaged model, the storage width ratio will be taken as 1, since we assume a rectangular cross-section that has no tidal flats. Of course, in many estuaries, tidal flats are present and the storage width ratio will be (far) above 1. Since r_s is of high influence for the Van der Burgh's coefficient due to the high power, this will lead to large uncertainties. Furthermore, parameters like the Chézy roughness, tidal

damping factor and density differences are hard to predict per estuary and will be taken as constants. So, when this method will be applied, a lot of estimations and simplifications have to be made, which causes high uncertainties and makes this method unsuitable for our salt intrusion prediction.

E Additional figures for results

Root Mean Square Error

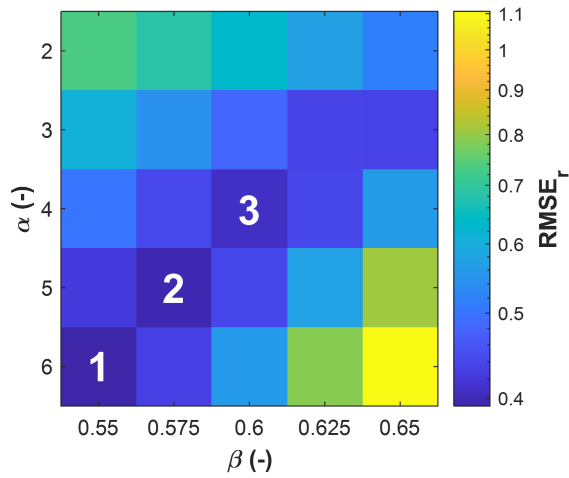


Figure 28: RMSE for river width ratio $B_{r,mod}/B_{r,obs}$, 1 to 3 indicates the top 3 lowest RMSE for the combinations of α and β .

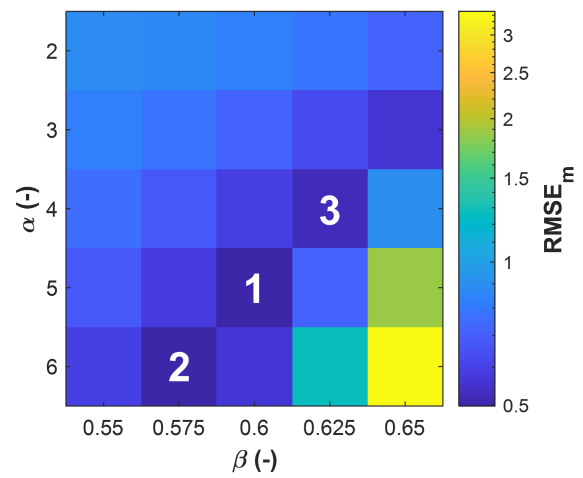


Figure 29: RMSE for mouth width ratio $B_{m,mod}/B_{m,obs}$, 1 to 3 indicates the top 3 lowest RMSE for the combinations of α and β .

Tidal excursion length

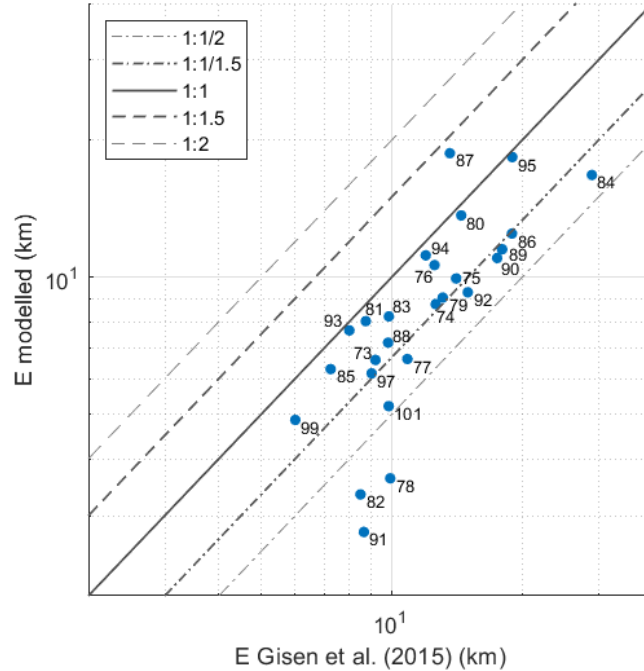


Figure 30: Tidal excursion length, only hydrodynamics from 1D tide-averaged model.

F Results for salt intrusion length and β_B and β_L

Table 4: The tide-dominance ratio I and salt intrusion length L^{HWS} for the yearly averaged river discharge for all estuaries. The exponent β_B in the river discharge-width relation and the exponent β_L for the river discharge-salt intrusion relation on the short term and long term for the estuaries of the data set by Nienhuis et al. (2018).

No.	Estuary	I	L^{HWS} (km)	β_B	β_L	β_L
		For $Q_{r,ave}$	For $Q_{r,ave}$	Long term	Short term	Long term
Estuaries of data set by Nienhuis et al. (2018)						
1	Amazon	2.42	307.3	0.165	0.499	0.326
2	Arno	0.22	1.5	0.471	0.477	0.112
3	Brazos	0.19	1.0	0.465	0.534	0.147
4	Ceyan	0.24	2.5	0.455	0.538	0.157
5	Chao Phraya	1.39	8.1	0.180	0.556	0.380
6	Colorado (MX)	11.52	74.1	0.064	0.413	0.289
7	Colorado (TX)	0.22	0.8	0.453	0.517	0.143
8	St George, Danube	0.02	0.4	0.561	0.684	0.154
9	Ebro	0.03	0.3	0.554	0.514	0.096
10	Eel	0.51	7.9	0.403	0.288	0.052
11	Fly	4.14	94.4	0.129	0.489	0.350
12	Fraser	5.41	80.3	0.125	0.435	0.273
13	Ganges/Brahmaputra	2.15	105.6	0.177	0.512	0.329
14	Godavari	0.52	12.5	0.333	0.578	0.243
16	Huanghe	0.35	6.6	0.317	0.612	0.306
17	Indus	6.62	91.0	0.107	0.423	0.270
18	Irrawaddy	3.45	106.1	0.154	0.476	0.305
19	Klamath	0.43	9.1	0.422	0.318	0.061
21	Kolyma	0.45	12.9	0.287	0.595	0.336
22	Krishna	0.72	13.2	0.247	0.576	0.313
23	Limpopo	0.65	8.5	0.258	0.581	0.313
24	Magdalena	0.18	4.3	0.445	0.613	0.202
25	Mahanadi	4.42	54.2	0.140	0.462	0.299
26	Mekong	0.74	19.4	0.221	0.582	0.369
27	Mississippi	0.07	2.6	0.504	0.651	0.185
28	Niger	2.25	48.5	0.163	0.505	0.318
29	Nile	0.14	4.3	0.436	0.634	0.254
30	Orange	0.58	7.0	0.351	0.539	0.208
31	Orinoco	0.64	47.3	0.268	0.574	0.333
32	Parana	0.24	13.6	0.385	0.609	0.279
33	Pechora	3.04	54.3	0.162	0.495	0.324
34	Pescara	0.14	1.0	0.507	0.357	0.047
35	Po	0.31	6.0	0.327	0.617	0.311
36	Rhone	0.16	3.5	0.470	0.611	0.185
37	Song Hong (Red River)	1.87	18.7	0.164	0.539	0.368
38	Squamish	0.47	7.8	0.414	0.275	0.041
39	Tigris-Euphrates	4.03	43.8	0.146	0.478	0.319
41	Vistula (Wisla)	0.22	2.3	0.449	0.561	0.172
43	Yangtze	3.05	139.3	0.157	0.487	0.316
44	Zhujiang (Pearl)	5.15	137.0	0.113	0.481	0.354
45	Pericama	209.83	140.4	0.004	0.177	0.061
46	Maracana	24.33	75.9	0.031	0.333	0.208
47	Marapanim	61.51	110.4	0.013	0.257	0.134
48	Cacipore	8.51	49.0	0.089	0.421	0.283
49	Suriname	3.55	22.4	0.128	0.472	0.301
50	Demerara	5.03	24.4	0.108	0.442	0.281
51	Sungai Merauke	6.22	30.7	0.112	0.442	0.294
52	Santa Lucia	0.19	5.5	0.460	0.591	0.181
53	Mahi	315.28	274.2	0.003	0.157	0.045
54	Narmada	134.66	314.8	0.006	0.181	0.058
55	Tapi	16.05	67.9	0.054	0.312	0.161
56	Purna	58.07	47.4	0.030	0.202	0.045

No.	Estuary	I	L^{HWS} (km)	β_B	β_L	β_L
		For $Q_{r,ave}$	For $Q_{r,ave}$	Long term	Short term	Long term
57	Hooghly	2.86	97.2	0.165	0.491	0.315
58	Kumbe	9.81	28.3	0.073	0.381	0.232
59	Yangon/Bago	4.75	83.0	0.127	0.472	0.326
60	Bilin	4.75	47.6	0.100	0.405	0.221
61	Thanlyin	5.27	105.1	0.114	0.472	0.337
62	Tanintharyi	5.89	55.1	0.108	0.473	0.346
63	Sungai Rokan	10.46	69.3	0.071	0.414	0.285
64	Sokyosen	65.68	176.1	0.014	0.187	0.048
65	Taeryong	17.41	80.8	0.050	0.309	0.161
66	Yoneshiro	0.15	1.4	0.458	0.624	0.198
67	Wai Bian	47.38	70.2	0.030	0.215	0.084
68	Weser	7.83	35.4	0.095	0.432	0.295
69	Thames	425.31	192.3	0.002	0.169	0.063
70	Ombrone	0.12	0.8	0.513	0.445	0.072
71	Tibre	0.14	1.0	0.501	0.498	0.112
72	Ord	252.67	91.8	0.005	0.148	0.023

Estuaries of data set by Gisen et al. (2015)

73	Kurau	15.53	48.7			
74	Perak	5.76	34.4			
75	Bernam	26.61	53.7			
76	Selangor	42.57	60.8			
77	Muar	17.66	52.1			
78	Endau	3.74	27.7			
79	Maputo	10.27	43.8			
80	Thames	2135.53	530.8			
81	Corantijn	7.25	38.2			
82	Sinnamary	0.44	7.6			
83	Mae Klong	9.09	28.8			
84	Lalang	28.65	49.8			
85	Limpopo	6.94	32.4			
86	Tha Chin	80.32	160.5			
87	Chao Phya	13.94	35.6			
88	Edisto	38.14	51.7			
89	Elbe	61.69	159.9			
90	Pangani	55.92	58.4			
91	Rembau Linggi	2.98	17.1			
92	Landak	108.82	51.5			
93	Delaware	20.20	76.8			
94	Westerschelde	98.24	240.5			
95	Pungue	40.30	121.2			
97	Solo	5.11	12.4			
98	Eems	44.41	86.2			
99	Tejo	8.82	35.3			
101	Ulu Sedili Besar	21.40	35.6			